

A resolution of the cosmic Lithium problem

Rachid Ouyed*

Department of Physics and Astronomy, University of Calgary, 2500 University Drive NW, Calgary, Alberta, T2N 1N4 Canada

15 April 2013

ABSTRACT

In 1982, Monique and François Spite discovered that the ${}^7\text{Li}$ abundance in the atmosphere of old metal-poor dwarf stars in the galactic halo was independent of metallicity and temperature. Since then, ${}^7\text{Li}$ abundance in the Universe has become a subject of intrigue, because there is less of it in Population II dwarf stars (by a factor of 3) than standard big bang nucleosynthesis predicts; a discrepancy which is still far from being solved. The most challenging features of the plateau is the lack of variability in the $-2.8 < [\text{Fe}/\text{H}] < -2.0$ metallicity range and the “meltdown” (a drop and an increase in variability) for $[\text{Fe}/\text{H}] < -2.8$. Here we show how quark-novae (QNe) occurring in the wake of Pop III stars, (a few days to a few weeks following the core-collapse SN explosions of $20\text{--}40M_{\odot}$ progenitors) can elegantly produce an $A(\text{Li}) \sim 2.2$ Lithium plateau in Pop II (low-mass) stars formed in the pristine cloud swept up by the mixed SN+QN ejecta. We also find an increase in the scatter as well as an eventual drop in $A(\text{Li})$ below the Spite plateau values for very low metallicity ($[\text{Fe}/\text{H}] < -3$) in excellent agreement with observations. We propose a solution to the discrepancy between the Big Bang Nucleosynthesis ${}^7\text{Li}$ abundance and the Spite plateau and list some implications and predictions of our model.

Key words: cosmology: theory – early universe – nuclear reactions, nucleosynthesis, abundances – supernovae: general – stars: carbon – stars: Population II, Population III

1 INTRODUCTION

One of the most important discoveries in the study of the chemical composition of stars was made in 1982 by Monique and François Spite, who found an essentially constant ${}^7\text{Li}$ abundance in warm metal-poor stars in the galactic Halo (Spite&Spite 1982). The lithium abundance shows a plateau with a near constant value¹ of $A(\text{Li}) \sim 2.2$ for metallicity between $[\text{Fe}/\text{H}] = -2$ and -2.8 (and effective stellar temperature $5900\text{ K} < T_{\text{eff}} < 6300\text{ K}$). The star-to-star scatter in ${}^7\text{Li}$ abundance in these stars is extremely small, of the order of ~ 0.05 dex (e.g. Asplund et al. 2006).

Given the low nuclear binding energy of ${}^7\text{Li}$ and because its cross section to proton capture is quite large, it needs only be exposed to relatively low stellar temperatures ($T \geq 2.5 \times 10^6\text{ K}$) to suffer substantial destruction over the many-billion-year life span of a halo star. These temperatures are never reached in the stellar atmospheres but if the convection zone is deep, ${}^7\text{Li}$ in the atmosphere is brought to hot deep layers where it is slowly destroyed. In warm ($T_{\text{eff}} \geq 5900\text{ K}$) metal-poor stars of Spite&Spite (1982) the convection is not so deep, and lithium should be preserved².

Therefore, the lithium abundance in the atmosphere of these stars is expected to reflect the abundance of ${}^7\text{Li}$ in the primitive Galactic matter; these stars hold the memory of the chemical composition of the interstellar medium or cloud from which they formed. It was proposed to identify the ${}^7\text{Li}$ abundance of the plateau to the abundance produced by the big bang (primordial lithium); i.e. as a relic of primordial nucleosynthesis³. However, several theoretical and observational results have cast doubt on use of the observed ${}^7\text{Li}$ plateau abundance as the primordial value despite its thinness (e.g. Ryan et al. 1999; Cyburt et al. 2008).

Thanks to high precision WMAP measurements of the cosmological constants (e.g. Dunkley et al. 2009; see also Larson et al. 2011; Komatsu et al. 2011), the Big Bang nucleosynthesis (BBN) of the elements (${}^3\text{He}$, ${}^4\text{He}$, D, ${}^6\text{Li}$ and ${}^7\text{Li}$) during the first few minutes in the evolution of the Universe, is now known with good precision. All elements occur in amounts predicted, except for ${}^7\text{Li}$. The corresponding primordial ${}^7\text{Li}$ abundance derived is $A(\text{Li}) = 2.72^{+0.05}_{-0.06}$ (Cyburt et al. 2008; Coc & Vangioni 2010), which is a factor of 3 times higher than the ${}^7\text{Li}$ abundance inferred from warm low-mass halo stars.

* email:rouyed@ucalgary.ca

¹ We adopt the standard definition $[A/B] = \log(N_A/N_B) - \log(N_A/N_B)_{\odot}$ and $A(\text{Li}) = \log(N_{\text{Li}}/N_{\text{H}}) + 12$ where the subscript \odot refers to solar values.

² In standard stellar models, the expected depletion of ${}^7\text{Li}$ for metal-poor turnoff stars is negligible, i.e., less than 0.02 dex (Deliyannis et al. 1990; Pinsonneault et al. 1992).

³ The mean value of the lithium abundance measured in the old galactic stars is also very close to the value measured in ω Cen cluster of $A(\text{Li}) = 2.19 \pm 0.14$ (see Bonifacio et al., 2010); presumably ω Cen is the remnant of a captured dwarf galaxy. This suggests that $A(\text{Li}) = 2.1\text{--}2.2$ could be a “universal value of stellar ${}^7\text{Li}$ abundance at low metallicity.

There are several discussions in the literature about how to solve this discrepancy between the measured Spite value and the WMAP/BBN results (e.g. Fields 2011 for a recent review). Ideas involve: (i) a first generation of primordial, zero-metallicity (Pop III), stars that has processed (by nuclear burning) and efficiently depleted lithium in a substantial fraction of the early halo baryonic matter before low-mass stars on the Spite plateau formed (Piau et al. 2006). This pre-galactic ${}^7\text{Li}$ processing idea faces some challenges; it does not appear to be able to explain the entire WMAP/Spite plateau gap (e.g. Sbordone et al. 2010). Furthermore, it appeals to Pop III stars with masses in the range $10\text{--}40M_{\odot}$ which are known to produce an amount of CNO elements much higher than the observed abundances in metal-poor halo stars (Prantzos 2007); (ii) Other theoretical studies involve non-standard BBN models exploring the frontiers of new physics (e.g. Jedamzik et al. 2006; Coc et al. 2009; Iocco et al. 2009; Jedamzik & Pospelov 2009; Kohri & Santos 2009). These modifications to the BBN consider the decay of unstable supersymmetric particles (e.g. Cyburt et al. 2010) to lower the primordial prediction. For e.g. if the late decaying particle is a gravitino, then the Spite plateau and the baryonic density determined by WMAP may be reconciled (e.g. Jedamzik et al. 2006). Non-standard BBN cannot explain the dependence of $A(\text{Li})$ on metallicity below $[\text{Fe}/\text{H}] \sim -2.8$; (iii) Studies involving modifications to the reaction cross-sections for the ${}^7\text{Li}$ production during BBN (e.g. Chakraborty, Fields & Olive 2011), although large errors in the cross section of the reaction leading to ${}^7\text{Li}$ are unlikely (e.g. Cyburt et al. 2004; Angulo et al. 2005). Ideas calling for alterations in ${}^7\text{Li}$ production reaction rates in nuclear physics and in particle physics in BBN have been ruled out as a cause (e.g. Coc et al. 2010); (iv) Alternatively, the discrepancy can in principle be eliminated by assuming that some degree of ${}^7\text{Li}$ depletion has occurred. Diffusion causes ${}^7\text{Li}$ (and other elements) to sink below the photosphere where it is destroyed at $T \geq 2 \times 10^6$ K by reactions with protons (e.g., Michaud et al. 1984; Salaris & Weiss 2001). The degree and efficiency of the photospheric depletion of ${}^7\text{Li}$ can be “controlled” by including mixing in diffusion models (e.g. Lambert 2004). For example, mixing due to Gravity waves (Talon et al. 2002; Charbonnel & Talon 2005), to Rotation (e.g., Vauclair 1988; Chaboyer & Demarque 1994; Pinsonneault et al. 2002; Talon & Charbonnel 2004) and, turbulence (Richard et al. 2005; Piau 2008). Richard et al. (2005) include a specific parametrization of turbulent mixing, and managed to produce a flat ${}^7\text{Li}$ abundance along the plateau, with $A(\text{Li})$ depleted by about 0.4 dex with respect to the initial value (see fig. 8 in Richard et al. 2005; see also Mucciarelli et al. 2011). The turbulence is included in these models without postulating any physical mechanism responsible for it and, its tuning leads to unwanted effects on the abundances of elements other than ${}^7\text{Li}$ (e.g. §6.4 in Bonifacio et al. 2007).

1.1 The challenge

The lithium problem is far from being solved. The puzzle remains the same and in some sense we are still facing severe problems in our understanding of how lithium was synthesized in the Big Bang and subsequently destroyed in stars. It is still unclear whether the disagreement results from lack of understanding of stellar lithium destruction mechanisms or from non-standard physics in BBN. Any new model must face two key questions (see discussion in Spite et al. 2012 and references in Fields 2011):

- **The very low scatter:** Based on data of the highest quality, there is very low scatter in the ${}^7\text{Li}$ abundances among stars on the ${}^7\text{Li}$ plateau; the actual scatter may even be smaller than the observed one (e.g. Asplund et al. 2006). The negligible scatter (≤ 0.05 dex), and apparent lack of slope in the Spite plateau are observational constraints, which ${}^7\text{Li}$ depletion models have trouble reproducing.

- **The meltdown:** The meltdown of the Spite plateau is established, but its cause is unclear (Sbordone et al. 2010). Specifically, below $[\text{Fe}/\text{H}] \sim -2.8$, more and more stars appear to exhibit ${}^7\text{Li}$ abundances below the plateau level, while scattering increasing. The challenge is to envision a single depletion phenomenon producing a thin, metallicity independent plateau above $[\text{Fe}/\text{H}] \sim -2.8$, and a highly scattered, metallicity dependent distribution below it.

The ${}^7\text{Li}$ problem has become increasingly acute and this “lingering” situation leaves room for new ideas to be explored. Here we appeal to primordial Quark-Novae (hereafter QNe) going-off in the wake of Pop III stars (prior to the era of Pop II stars). The core-collapse (Type-II) SN explosion of a Pop III star with mass in the $20M_{\odot} < M_{\text{prog.}} < 40M_{\odot}$ range would leave behind a neutron star massive enough to experience an explosive transition to a quark star; the QN (Ouyed et al. 2002; Vogt et al. 2004; Ouyed et al. 2005; Keränen et al. 2005; Niebergal et al. 2010). A QN explosion ejects the neutron-rich outer layers of the parent neutron star. This ejecta expands away from the quark star (the compact remnant) at relativistic speeds with an average Lorentz factor $\Gamma_{\text{QN}} \approx 10$; i.e. a typical neutron energy $E_{\text{QN}} = 10$ GeV (Keränen et al. 2005; Ouyed et al. 2005). The interaction between the neutron-rich QN ejecta and the preceding (Pop III) type-II SN ejecta leads to spallation products with abundances reflective of extremely metal-poor stars (Ouyed 2013). Spallation (i.e. destruction) of the ${}^{56}\text{Ni}$ in the ejecta of the (Pop III) type II SN by the QN neutrons leads to iron-impoverishment in the cloud swept up by the combined SN+QN ejecta. The Pop II stars formed in these clouds will appear metal-poor with $[\text{Fe}/\text{H}]$ decreasing with t_{delay} (the time delay between the SN explosion and the subsequent QN explosion; see Figure 1 in Ouyed 2013). In this paper, we focus mainly on ${}^7\text{Li}$ production in these primordial QNe and extend the work of Ouyed (2013) by considering a more complete element composition in the (Pop III) type-II SN ejecta. We show that a QN can produce an ${}^7\text{Li}$ plateau with values matching Spite levels of $A(\text{Li}) \sim 2.2$ and, with features satisfying the criteria set out above.

The paper is organized as follows. In Section 2 we briefly present the QN model, primordial QNe and discuss their progenitors. We give a brief overview of the QN model and of primordial QNe occurring in the wake of Pop III stars; i.e. QNe from the explosions of massive neutrons stars left behind by core-collapse of stars at the lower mass end ($20M_{\odot} < M_{\text{prog.}} < 40M_{\odot}$) of the Pop III mass distribution. Section 3 describes our model’s parameters and its general features including ${}^{56}\text{Ni}$ destruction by QN neutrons and the resulting Fe impoverishment in the pristine clouds swept up by primordial QNe. Here we discuss the resulting sub-Fe spallation products and the α -elements and compare our findings to observations. When necessary the interested reader will be referred to Ouyed et al. (2011) and Ouyed (2013) for more details on the spallation process, numerical procedure, and relevant references. Section 4 focuses entirely on ${}^7\text{Li}$ production and describes how a low-scatter, $A(\text{Li}) \sim 2.2$, plateau is obtained in our model. A discussion and predictions are given in Section 5 before we conclude in Section 6.

2 PRIMORDIAL QUARK-NOVAE

The basic picture of the QN is that a massive neutron star (NS; with $M_{\text{NS}} > 1.6M_{\odot}$) converts explosively to a quark star. Such an explosion can happen if the massive NS, in its spin-down evolution or via mass accretion (e.g. from fall-back material), reaches the quark deconfinement density in its core (Staff et al. 2006) and subsequently undergoes a phase transition to the conjectured more stable strange quark matter phase (Itoh 1970; Bodmer 1971; Witten 1984; see also Terazawa 1979). This results in a strange quark matter conversion front that propagates toward the surface of the NS with a detonation occurring before the surface is reached (Keränen et al. 2005; Niebergal et al. 2010). The outcome of the QN explosion – besides the formation of a quark star – is the ejection of the NS’s outermost layers (a very neutron-rich ejecta with an average mass $M_{\text{QN}} \sim 10^{-3}M_{\odot}$) at relativistic speeds (with a Lorentz factor averaging $\Gamma_{\text{QN}} \sim 10$; Ouyed&Leahy 2009). The outer layers are ejected from an expanding thermal fireball (Vogt et al. 2004; Ouyed et al. 2005) which allows for ejecta with kinetic energy, $E_{\text{QN}}^{\text{KE}} > 10^{52}$ erg. Hereafter we assume that a typical neutron in the QN ejecta will be streaming out with energy $E_{\text{QN}} \simeq 10$ GeV; not to be confused with the total ejecta’s kinetic energy $E_{\text{QN}}^{\text{KE}}$. This means that the $M_{\text{QN}} \sim 10^{-3}M_{\odot}$ QN ejecta will have a typical total kinetic energy of $E_{\text{QN}}^{\text{KE}} \sim 2 \times 10^{52}$ erg.

2.1 Dual-shock Quark Novae (dsQNe)

When the QN occurs a few days to a few weeks following the preceding Type II SN (SNII) explosion, a dual-shock QN (hereafter dsQNe) is created. The interaction between the relativistic, neutron-rich, QN ejecta (Keränen et al. 2005; Ouyed&Leahy 2009) and the SNII ejecta leads to spallation of the SN material. This time delay, t_{delay} , plays a crucial role in our model since it defines the density of the expanding SN ejecta (and thus spallation efficiency) when it is hit by the $E_{\text{QN}} \sim 10$ GeV QN neutrons (the primaries in our model; see §3.1 below). If the time t_{delay} between SN and QN explosions is lengthy, the SN ejecta will have dissipated such that the QN essentially erupts in isolation. However, when t_{delay} is on the order of days to weeks the neutron-rich QN ejecta interacts with the preceding SN ejecta leading to unique spallation products (Ouyed et al. 2011; Ouyed 2013).

2.2 The Pop III Type-II SN (PopIII-SNII) progenitor

Studies of star formation in the early Universe suggest that the first stars (Pop III) were typically more massive than present day objects, with $100M_{\odot}$ for zero metallicity (Z) objects (Abel et al. 2002; Nakamura & Umemura 2002; Bromm&Larson 2004; Loeb et al. 2008). The progenitors of QNe are stars with masses in the $20M_{\odot} < M_{\text{prog.}} < 40M_{\odot}$ range (e.g. Ouyed et al. 2009a; Ouyed et al. 2009b; Leahy&Ouyed 2009; Ouyed&Leahy 2012; Ouyed 2013). Thus, primordial QNe are expected to occur in the wake of these Pop III stars from progenitors with mass range at the lower end of the mass distribution; $20M_{\odot} < M_{\text{prog.}} < 40M_{\odot}$. These are expected to explode as TypeII SNe and would most likely form NSs massive enough to result in QNe once quark deconfinement density is reached in their cores (Staff et al. 2006). Hereafter we refer to them as PopIII-SNII progenitors.

3 OUR MODEL

In this section, we summarize and discuss our model’s parameters and its general features and present some results. In all of our calculations we divide the target layer into N_{mfp,A_T} sublayers of radial thickness equivalent to a spallation mean-free-path (mfp), λ_{sp,A_T} . In each mfp of interaction, a given A_T nucleus will be hit multiple times by neutrons. To produce a realistic distribution of product nuclei from this sub-layer, we draw the number of hits from a poisson distribution. As shown in Ouyed et al. (2011), a Poissonian description is appropriate since we have a small spallation cross section but a rapidly increasing number of hits due to the cascading effect as more neutrons and protons are created. The interested reader is referred to Ouyed et al. (2011; see eqs 3, 4 and 5 in that paper) and Ouyed (2013) for more details on the spallation process, numerical procedure, and relevant references.

3.1 Model Parameters

We start by summarizing the key parameters in our model:

- **The PopIII-SNII ejecta’s composition:** Studies of the chemical composition of PopIII-SNII ejecta in the $20M_{\odot} < M_{\text{prog.}} < 40M_{\odot}$ mass range can be found in the literature for mixed and unmixed SN ejecta (Umeda&Nomoto 2002; Nozawa et al. 2003; Cherchneff&Dwek 2009; Heger& Woosley 2010). Among the main products of these PopIII-SNII supernovae are ^{56}Ni , ^{32}S , ^{28}Si , ^{24}Mg , ^{20}Ne , ^{16}O and, ^{12}C . Other elements (including ^{14}N ; see §3.3 below) are present at much smaller levels so we ignore them here. We also ignore elements heavier than ^{56}Ni in the present study. While some differences exist in mass yields between different groups, and between models with mixing and non-mixing, we find that a typical $20M_{\odot}$ PopIII-SN ejecta (with 10^{51} erg in energy) can be represented with mass yields $M_{\text{Ni,SN}} \sim 0.1M_{\odot}$, $M_{\text{S,SN}} \sim 0.05M_{\odot}$, $M_{\text{Si,SN}} \sim 0.05M_{\odot}$, $M_{\text{Mg,SN}} \sim 0.05M_{\odot}$, $M_{\text{Ne,SN}} \sim 0.05M_{\odot}$, $M_{\text{O,SN}} \sim 1.5M_{\odot}$, $M_{\text{C,SN}} \sim 0.15M_{\odot}$. We adopt these values as initial, fiducial, values for the target material; i.e. the PopIII-SN ejecta in our model.

Although some mixing is likely to occur during the PopIII-SNII explosions, here we assume an onion-like profile of the expanding SN ejecta (i.e., no mixing) with the innermost ejecta, viz., ^{56}Ni nuclei (mass number $A_T=56$) constituting the target A_T at a distance $R_{A_T}(t_{\text{delay}})=v_{\text{sn}} t_{\text{delay}}$ from the center of the explosion; we assume v_{sn} to be constant since the QN occurs while the SN ejecta is still in the Sedov phase (e.g., McCray 1985). Carbon (^{12}C) makes up the last layer in this onion-like geometry overlaying the Oxygen layer. The ^4He and H layers overlaying the carbon layer can be ignored since in most cases considered here we find that the spallation mean-free-path of the (primary, secondary and subsequent generations of) neutrons always exceeds the (H and ^4He) layers’ thickness.

- **The time delay (t_{delay}):** The number density in the target layer (made of element A_T) is defined as $n_{A_T} = M_{A_T,\text{SN}} / (4\pi R_{A_T}^2 \Delta R_{A_T} A_T m_H)$ where $M_{A_T,\text{SN}}$ is the mass of the layer (the target’s initial mass in the PopIII-SN ejecta prior to impact by the QN neutrons), ΔR_{A_T} the layer’s thickness and $R_{A_T} = v_{\text{sn}} t_{\text{delay}}$ the radius of the layer from the center of the SN explosion; m_H is the hydrogen mass. For a given PopIII-SNII explosion with known $M_{A_T,\text{SN}}$ (e.g. for a fixed amount of ^{56}Ni processed during the explosion) and given v_{sn} which remains constant early in the expansion of the SN ejecta, t_{delay} becomes the key parameter that defines the target density; i.e. the longer the time delay, t_{delay} , the lower the target density when it is hit by the relativistic QN neutrons.

Table 1. Average multiplicity (ζ) and energy of spallated neutrons for dsQNe with $t_{\text{delay}} = t_{\text{outer}} \sim 8.3$ days; this is the regime where the QN neutrons interact with the innermost layers (^{56}Ni , ^{32}S , ^{28}Si). For this time delay, $N_{\text{mfp},A_T} \sim 1$ which means that the thickness of each target layer is equivalent to roughly one spallation mfp (see eq. 1). Spallation stops at the ^{28}Si layer since the subsequent generation of neutrons exit the ^{32}S layer with energies ~ 0.15 GeV which is below critical for spallation to ensue in the overlaying layers ^{24}Mg layer ($E_{\text{sp},\text{Mg}} \sim 0.18$ GeV; see discussion following eq. 2).

A_T	Primaries ($E_0 = E_{\text{QN}} = 10$ GeV)			Primaries ($E_0 = E_{\text{QN}} = 5$ GeV)		
	^{56}Ni	^{32}S	^{28}Si	^{56}Ni	^{32}S	^{28}Si
$\zeta_{\text{av},i}$	~ 13.1	~ 3.6	~ 1.4	~ 11.3	~ 2.8	~ 1.1
$E_{\text{av},i} = \frac{\zeta_{\text{av},i-1}}{\zeta_{\text{av},i}}$ (GeV)	~ 0.77	~ 0.21	~ 0.15	~ 0.44	~ 0.16	~ 0.15
$^\dagger A_{\text{peak},i} \approx A_T - \zeta_{\text{av},i}$	$\sim ^{44}\text{Ti}$	$\sim ^{48}\text{Si}$	$\sim ^{27}\text{Al}$	$\sim ^{45}\text{Sc}$	$\sim ^{28}\text{Si}$	$\sim ^{27}\text{Al}$
$^\ddagger \zeta_{\text{net},i} = \zeta_{\text{av},i-1} \times \zeta_{\text{av},i}$	~ 13.1	~ 47.2	~ 66	~ 11.3	~ 31.7	~ 34.8

† The resulting spallation products would acquire a normal distribution peaking at atomic weight $A_{\text{peak},i} \sim A_T - \zeta_i$.

‡ The net multiplicity (ζ_{net} ; see eq. 4 in Ouyed 2013) translates to a total spallation neutrons and protons which amounts to $M_{\text{n+p}} = \zeta_{\text{net}} M_{\text{QN}} \sim 0.05\text{--}0.1 M_\odot$.

Table 2. Average multiplicity (ζ) and energy of spallated neutrons in the oxygen (^{16}O) layer for dsQNe with $t_{\text{delay}} > t_{\text{outer}}$ (here $t_{\text{delay}} = 12$ days); this is regime where the QN neutrons barely interact with the inner layers and proceed directly to the oxygen layer. The thickness of the oxygen layer (with $M_{\text{O,SN}} = 1.5 M_\odot$) is equivalent to $N_{\text{sp},\text{O}} \sim 10$ sub-layers each of radial thickness or the order of a spallation mfp (see eq. 1). Spallation in the oxygen layer ceases when the neutron energy is below the threshold value for O-spallation ($E_{\text{sp},\text{O}} \sim 0.27$ GeV) or when the neutrons run out of target material (i.e. after $N_{\text{sp},\text{O}} \sim 10$ mfps).

	Primaries ($E_0 = E_{\text{QN}} = 10$ GeV)					Primaries ($E_0 = E_{\text{QN}} = 5$ GeV)				
	mfp 1	mfp 2	mfp 3	mfp 4	mfp 5	mfp 1	mfp 2	mfp 3	mfp 4	mfp 5
$\zeta_{\text{av},i}$	~ 3.8	~ 2.7	~ 2	~ 1.5	~ 1.1	~ 3.2	~ 2.4	~ 1.7	~ 1.3	~ 1.1
$E_{\text{av},i} = \frac{\zeta_{\text{av},i-1}}{\zeta_{\text{av},i}}$ (GeV)	~ 2.7	~ 1.0	~ 0.5	~ 0.34	~ 0.28	~ 1.6	~ 0.7	~ 0.4	~ 0.3	~ 0.28
$^\dagger A_{\text{peak},i} \approx 16 - \zeta_{\text{av},i}$	^{12}C	^{13}C	^{14}N	^{14}N	^{15}O	^{13}C	^{14}N	^{14}N	^{15}O	^{15}O
$^\ddagger \zeta_{\text{net},i} = \zeta_{i-1} \times \zeta_i$	~ 3.8	~ 10.3	~ 20.6	~ 31	~ 34	~ 3.2	~ 7.7	~ 13	~ 17	~ 19

† The resulting spallation products would acquire a normal distribution peaking at atomic weight $A_{\text{peak},i} \sim 16 - \zeta_i$.

‡ The net multiplicity (ζ_{net} ; see eq. 4 in Ouyed 2013) translates to a total spallation neutrons and protons which amounts to $M_{\text{n+p}} = \zeta_{\text{net}} M_{\text{QN}} \sim 0.02\text{--}0.04 M_\odot$.

The neutron spallation mean-free path (mfp) on a target A_T is $\lambda_{\text{sp},A_T} = 1/(n_{A_T} \sigma_{\text{sp},A_T})$ where the spallation cross section in millibarns is $\sigma_{\text{sp},A_T} = 45A_{A_T}^{0.7}$ mb (see Ouyed et al. 2011). The average number of collisions (i.e. the number of spallation mfps) an incoming neutron experiences in the target layer A_T is

$$N_{\text{mfp},A_T} \approx \frac{\Delta R_{A_T}}{\lambda_{\text{sp},A_T}} \approx 0.69 \frac{M_{A_T,\text{SN}}/0.1 M_\odot}{(A_{T,56})^{0.3} (v_{\text{sn},5000} t_{\text{delay},10})^2}, \quad (1)$$

where $A_{T,56}$ is the target atomic mass in units of 56 and $0.1 M_\odot$ representative of the mass in the ^{56}Ni layer. In the equation above, v_{sn} is given in units of 5000 km s^{-1} and is kept constant in all of the simulations shown in this paper. The time delay, t_{delay} , is in units of 10 days. For our fiducial values in mass of the target material and for $t_{\text{delay}} = 10$ days we get $N_{\text{mfp},\text{Ni}} \sim 0.69$, $N_{\text{mfp},\text{S}} \sim 0.41$, $N_{\text{mfp},\text{Si}} \sim 0.42$, $N_{\text{mfp},\text{Mg}} \sim 0.44$, $N_{\text{mfp},\text{Ne}} \sim 0.47$, $N_{\text{mfp},\text{O}} \sim 15.10$, $N_{\text{mfp},\text{C}} \sim 1.64$ for spallation on ^{56}Ni , ^{32}S , ^{28}Si , ^{24}Mg , ^{20}Ne , ^{16}O , ^{12}C , respectively.

In a regime where $\lambda_{\text{sp},A_T} > \Delta R_{A_T}$ (i.e. $N_{\text{mfp},A_T} < 1$), there will be minimal or no spallation induced by the QN neutrons on the target A_T and the neutrons proceed onto the next, overlaying, layer. Thus, for a given $M_{A_T,\text{SN}}$ and v_{sn} this defines a critical time delay above which no spallation occurs in layer of element A_T . This allows us to define four regimes in our model: (i) $t_{\text{delay}} > t_{\text{outer}}$ with minimal or no spallation occurring in the inner layers. It means that for $t_{\text{delay}} > t_{\text{outer}} \approx 8.3 \text{ days} \times (M_{\text{Ni,SN}}/0.1 M_\odot)^{1/2} / (A_{T,56}^{0.15} v_{\text{sn},5000})$ days (see eq. 2 in Ouyed 2013), the QN neutrons barely interact with the inner layers and proceed directly to the outer (O and C layers); (ii) $t_{\text{delay}} < t_{\text{inner}}$ with spallation occurring mainly in the inner layers, beneath the oxygen layer, with $t_{\text{inner}} \approx 6.3 \text{ days} \times$

$(M_{\text{Ni,SN}}/0.1 M_\odot)^{1/2} / (A_{T,56}^{0.15} v_{\text{sn},5000})$ (see Eq. 6 in Ouyed 2013)⁴. This regime corresponds to the situation where the spallated (i.e. subsequent generations of) neutrons exiting the inner layers, do not have enough energy to spallate the outer CO-rich layers; (iii) $t_{\text{inner}} < t_{\text{delay}} < t_{\text{outer}}$ with spallation occurring both in the inner and outer layers. In this regime, the neutrons spallated in the inner layers end up with energies above the critical values for spallation in the ^{16}O (and in certain cases in the ^{12}C) to ensue; (iv) $t_{\text{delay}} > t_{\text{no-spall}}$ which effectively defines a regime of a QN occurring in isolation since no interaction occurs between the SN and QN ejecta. For our fiducial values, $t_{\text{no-spall}} \sim 23\text{--}24$ days. For $t_{\text{outer}} < t_{\text{delay}} < t_{\text{no-spall}}$, spallation would occur mainly in the oxygen and carbon layers.

• **The energy per nucleon, E_{QN} , in the neutron-rich QN ejecta:** It defines and sets the total multiplicity, ζ , of the spallated (i.e. subsequent generations of) neutrons and protons and their energies. The average neutrons+proton multiplicity ζ_{av} on target A_T is given in eq. (2) in Ouyed (2013) as

$$\zeta_{\text{av}} \approx 7A_{A_T,56} \times (1 + 0.38 \ln E_n), \quad (2)$$

where E_n is the neutron energy in GeV which leads to a subsequent generation of spallated neutrons and protons with energy $\sim E_n/\zeta_{\text{av}}$. The resulting spallation product's atomic weight will peak at $A_T - \zeta_{\text{av}}$. The $\zeta_{\text{av}} > 1$ condition gives the minimum neutron energy necessary for spallation to occur in the Ni, S, Si, Mg, Ne, O, C layer to be $E_{\text{sp},A_T} \sim 0.105, 0.139, 0.153, 0.173, 0.206, 0.268, 0.416$ GeV, respectively.

⁴ In Ouyed (2013), t_{outer} and t_{inner} were defined as t_{Ni} and t_{O} , respectively.

Table 1 shows results from simulations involving the interaction of $E_{\text{QN}} = 5$ GeV and $E_{\text{QN}} = 10$ GeV neutrons with the PopIII-SNII ejecta when $t_{\text{delay}} = t_{\text{outer}} \approx 8.3$ days. For our fiducial values of the targets' initial masses this time delay implies $N_{\text{mfp,Ni}} \sim N_{\text{mfp,S}} \sim N_{\text{mfp,Si}} \sim N_{\text{mfp,Mg}} \sim N_{\text{mfp,Ne}} \sim 1$ which means that on average a QN neutron will interact once per layer. An $E_0 = E_{\text{QN}} = 10$ GeV QN (primary) neutron would lead to a multiplicity of $\zeta_{\text{av.}} \sim 13$ in the ^{56}Ni layer. This means a spallated (secondary generation of) neutrons and protons exiting the layer with energy $E_1 = E_0/\zeta_{\text{av.}} \sim 0.77$ GeV. These secondary nucleons induce an average multiplicity $\zeta_{\text{av.}} \sim 3.6$ in the ^{32}S layer which yields spallated (tertiary generation of) neutrons and protons exiting the layer with energy ~ 0.21 GeV. As can be seen from Table 1, spallation ceases at the Si layer since within the first three layers the neutrons energy has cascaded down to ~ 0.15 GeV, below the critical value for Mg-spallation. The main (i.e. peak) spallation products are shown as well as the net multiplicity ζ_{net} which yields a total mass of spallated neutrons and protons which amounts to $M_{\text{n+p}} = \zeta_{\text{net}} M_{\text{QN}} \sim 0.05\text{--}0.1 M_{\odot}$. This table shows the pathway of a typical neutron with the expected average multiplicity given by eq. (2). However, because the ζ distribution is not uniform, some neutrons induce above average multiplicity ($\zeta > \zeta_{\text{av.}}$) and stop within the ^{56}Ni layer while those inducing below average multiplicity ($\zeta < \zeta_{\text{av.}}$) make it past the inner layers and induce spallation in the oxygen layer (see discussion below).

Another example is shown in Table 2 which shows results from the interaction of $E_{\text{QN}} = 5$ GeV and $E_{\text{QN}} = 10$ GeV neutrons with the PopIII-SNII ejecta when $t_{\text{delay}} > t_{\text{outer}}$ (here $t_{\text{delay}} = 12$ days). For our fiducial values, $N_{\lambda_{\text{sp.,O}}} \sim 10$ and $E_{\text{sp.,O}} \sim 0.27$ GeV. As can be seen from Table 2, neutrons interact with five sub-layers (each representing a spallation mfp) before their energy cascade down below 0.268 GeV. Thus half the amount of oxygen in the PopIII-SNII will be destroyed forming sub-O products. In each sub-layer denoted by index i (i.e. for each mfp, or $\lambda_{\text{sp.,O}}$), the atomic weight of the spallation products is close to a normal distribution peaking at atomic weight $A_{\text{peak},i} \sim A_{\text{T}} - \zeta_{\text{av.,i}}$. The final abundances of the spallation products is a combination of these distributions (see Figure 1 in Ouyed et al. 2011). As can be seen in Table 2 the total spallation neutrons and protons amounts to $M_{\text{n+p}} = \zeta_{\text{net}} M_{\text{QN}} \sim 0.02\text{--}0.04 M_{\odot}$. This Table further illustrates the important point that most of the spallated neutrons exiting the oxygen layer will not be able to induce spallation in the overlaying C layer since their energy is below the threshold for C-spallation (~ 0.42 GeV). See however discussion below.

We end this subsection by mentioning some important points:

(i) The true ζ distribution is not uniform and is rather close to a normal distribution peaking at $\zeta_{\text{av.}}$. This means that the spallated neutrons would exit a sub-layer i of the target material (A_{T}) with a non-uniform energy distribution peaking at $\sim E_i/\zeta_{\text{av.,i}}$. For the case shown in Table 2, most of the neutrons spallated in the oxygen layer will not be able to induce spallation in the overlaying C layer – since their energy is below the threshold for C-spallation $E_{\text{sp.,C}} \sim 0.42$ GeV. However, neutrons leading to a multiplicity $\zeta < \zeta_{\text{av.}}$ do induce spallation after exiting the oxygen layer. As we show later (see §4.1.1), this has important consequences to production of ^7Li from spallation in the C-layer;

(ii) The logarithmic energy dependence of $\zeta_{\text{av.}}$ means that there is little difference between the multiplicity distribution induced by the $E_{\text{QN}} = 10$ GeV and the $E_{\text{QN}} = 5$ GeV neutrons. However, for the lower energy primaries with $E_0 = E_{\text{QN}}$ (i.e. QN neutrons), the resulting average energy per spallated nucleon is lower. In the case of spallation in the Oxygen layer for example (as illustrated in Table 2), the $E_{\text{QN}} = 5$ GeV simulations shows fewer neutrons with

energy above $E_{\text{sp.,C}} \sim 0.42$ GeV making it past the oxygen layer; i.e. spallation in the overlaying C-layer is reduced as compared to the $E_{\text{QN}} = 10$ GeV simulations (discussed further in §4.1.1);

(iii) Even if the spallation condition, $E_n > E_{\text{sp.,AT}}$, is satisfied in any layer of target material A_{T} (a necessary condition), it is not sufficient when $\lambda_{\text{sp.,AT}} > \Delta R_{\text{AT}}$; i.e. when the spallation mfp exceeds the thickness of the target layer (see discussion following eq. 1). Thus the $E_n > E_{\text{sp.,AT}}$ and the $\Delta R_{\text{AT}} > \lambda_{\text{sp.,AT}}$ must be satisfied simultaneously.

3.2 ^{56}Ni destruction and Iron-impooverishment in our model

3.2.1 The t_{delay} -[Fe/H] connection

Following spallation in the ^{56}Ni layer, the resulting iron abundance ([Fe/H]) in the primordial cloud swept by the combined SN+QN ejecta is (eq. 5 in Ouyed 2013):

$$\left[\frac{\text{Fe}}{\text{H}} \right] = \log \eta_{56}^{56} + \log \frac{M_{\text{Ni,SN}}/0.1 M_{\odot}}{M_{\text{sw}}/10^5 M_{\odot}} - 3.12, \quad (3)$$

where $\eta_{\text{A}}^{\text{AT}} = M_{\text{A}}/M_{\text{AT,SN}}$ is the normalized mass yields of product/element A following spallation on target A_{T} (originally present in the SN ejecta; here 56 refers to ^{56}Ni). Here M_{sw} is the mass swept up by the mixed SN+QN ejecta in the primordial pristine cloud surrounding the site of the dsQN explosion; M_{sw} is in units of $10^5 M_{\odot}$ (e.g. Shigeyama&Tsujimoto 1998; Machida et al. 2005).

In our model, a dsQN with a given t_{delay} translates to a corresponding [Fe/H] abundance in the swept up cloud; this is set by the parameter η_{56}^{56} which is the level of depletion of the original PopIII-SNII ^{56}Ni following spallation. Figure 1 in Ouyed (2013) shows the heavy depletion of the original PopIII-SNII ^{56}Ni by spallation obtained for very short time delays ($t_{\text{delay}} < 2$ days) where $\eta_{56}^{56} < 10^{-4}$ (i.e. leading to $[\text{Fe}/\text{H}] < -7$). Hyper metal-poor stars (HMPs with $[\text{Fe}/\text{H}] < -5$ in the terminology of Beers&Christlieb 2005) would form from clouds swept up by $t_{\text{delay}} < 3$ days dsQNe in our model (see §5).

In dsQNe with long enough delays (i.e. $t_{\text{delay}} > t_{\text{outer}}$), there is minimal spallation in the ^{56}Ni layer (i.e. $\eta_{56}^{56} \approx 1$) and in the innermost layers (^{32}S , ^{28}S , ^{24}Mg) layers. For such dsQNe, high values of [Fe/H] are obtained by increasing $M_{\text{Ni,SN}}$ or by decreasing the amount of swept up material, M_{sw} (see eq. 3 above). For example, a dsQN with $t_{\text{delay}} > 10$ days, $M_{\text{Ni,SN}} = 0.5 M_{\odot}$ and $M_{\text{sw}} = 10^{4.5} M_{\odot}$ gives $[\text{Fe}/\text{H}] \sim -1.9$.

3.2.2 Sub-Fe elements

Shown in Figure 1 in this paper are abundances of sub-Fe spallation products resulting from dsQNe with different t_{delay} ; shown is the relative abundance $[X/\text{Fe}]$. The original composition of the PopIII-SNII ejecta is shown by the plus signs in all of the panels. These elements are identified by an asterix next to their names in all of the panels as their abundances vary with t_{delay} .

For $t_{\text{delay}} > t_{\text{no-spall}} \sim 23\text{--}24$ days (not shown here) no spallation occurs and the original elements (identified with an asterix) fall exactly on the plus signs. For $t_{\text{outer}} \sim 8.3$ days $< t_{\text{delay}} < t_{\text{no-spall}}$, there is minimal interaction in the inner layers and most spallation products are light elements from O- and C-spallation. The original relative abundance of the PopIII-SNII elements is almost conserved except for some spallation in the oxygen layer which leads to the formation of B, Be and Li. For intermediate t_{delay} (i.e. $t_{\text{inner}} \sim 6.3$ days $< t_{\text{delay}} < t_{\text{outer}}$), spallation occurs in almost all of

the layers. As t_{delay} gets shorter spallation efficiency start to decrease in the outer layers and eventually for $t_{\text{delay}} < \sim 6$ days spallation starts to become more prominent in the innermost layers. For even shorter t_{delay} (top panels), most of the QN neutrons are used up in the ^{56}Ni layer thus shielding all of the overlaying layers. Effectively, the original PopIII-SNII sub-Ni elements (S, Si, Mg, Ne, O, C) present in the PopIII-SNII ejecta would be preserved in dsQNe with very short delays. In addition these elements will be produced as by-products of spallation in the ^{56}Ni layer which further increases their overall $[X/\text{Fe}]$ values for $t_{\text{delay}} < 3$ days. The weak-dependency of multiplicity on the neutrons' energy explains the nearly similar final abundances for the $E_{\text{QN}} = 5$ GeV and the $E_{\text{QN}} = 10$ GeV simulations.

3.2.3 α -elements

The so-called α -elements (O, Ne, Mg, Si, S, Ca, Ti) in very metal-poor stars are reported to be overabundant relative to iron at low metallicity (e.g. McWilliam 1997; Aoki et al. 2007) with $[\alpha/\text{Fe}] > [\alpha/\text{Fe}]_{\odot}$ where $[\alpha/\text{Fe}] = \frac{1}{4}([Mg/\text{Fe}] + [Si/\text{Fe}] + [Ca/\text{Fe}] + [Ti/\text{Fe}])$ (the average abundance of Mg, Si, Ca and Ti). These enhancements increase linearly with decreasing metallicity.

Figure 2 shows the relative abundances of the original PopIII-SNII elements with respect to t_{delay} (top panel) and metallicity (lower panel) for simulations with $E_{\text{QN}} = 5$ GeV. Figure 3 shows the results for the $E_{\text{QN}} = 10$ GeV simulations. For $t_{\text{delay}} > t_{\text{outer}} \sim 8.3$ days, $[X/\text{Fe}]$ remain close to the original values except for oxygen which experiences some spallation and thus depletion up to $t_{\text{delay}} \sim 15$ days since it is by far the most abundant PopIII-SNII element. For $t_{\text{inner}} < t_{\text{delay}} < t_{\text{outer}}$, spallation occurs in most of the PopIII-SNII layers leading to an overall reduction in the abundances of the original elements. This leads to a dip in the $[X/\text{Fe}]$ values in Figure 2 and in Figure 3 for $-4 < [\text{Fe}/\text{H}] < -3$. A plateau-like behaviour is noticeable in the dip for all of the PopIII-SNII elements. The $[\text{Si}/\text{Fe}]$ and $[\text{Mg}/\text{Fe}]$ levels in the dip region, combined with the copious production of Ti and Ca from Ni-spallation (see Figure 1) lead to $[\alpha/\text{Fe}] > [\alpha/\text{Fe}]_{\odot}$ in our model and in particular for $t_{\text{delay}} < t_{\text{outer}} \sim 8.3$ days (i.e. $[\text{Fe}/\text{H}] < -3$) since spallation is more pronounced in the ^{56}Ni layer than in the overlaying layers.

An increase of $[X/\text{Fe}]$ is evident for most elements when the metallicity decreases below ~ -4 ; i.e. when t_{delay} decreases below roughly 5 to 6 days. These layers are shielded at the expense of ^{56}Ni depletion explaining the increase in $[X/\text{Fe}]$ much above the initial values. In general, and for short t_{delay} in our model, the more abundant a specific element is in the PopIII-SNII shocked ejecta, prior to spallation by the QN neutrons, the more it will appear abundant following the destruction of ^{56}Ni (i.e. the reduction of the final iron abundance in the swept up cloud). Since O and C are the two-most abundant elements in the PopIII-SNII ejecta, it is no surprise that $[\text{C}/\text{Fe}]$ and $[\text{O}/\text{Fe}]$ are very enhanced for very short delays (see below for the special case of ^{32}S). These enhancement would be reflected in the composition of the gas cloud swept up by the SN+QN ejecta out of which the Pop II low-mass stars would form.

3.2.4 Sulfur

Figures 2 and 3 show that Sulfur is more depleted (with $[\text{S}/\text{Fe}]$ showing the lowest plateau in the dip) than the other original elements in the PopIII-SNII ejecta for $6.3 \text{ days} < t_{\text{delay}} < 8.3 \text{ days}$ (i.e. $-4 < [\text{Fe}/\text{H}] < -3$) due to its close proximity to the Nickel layer.

Even for very short delays, because of the non-uniform distribution in multiplicity ζ , some spallated neutrons in the ^{56}Ni manage to make it to the overlaying ^{32}S layer. This explains why the ^{32}S plateau in the dip extends to metallicity as low as $[\text{Fe}/\text{H}] \sim -4$. Only for $t_{\text{delay}} < 5$ days (i.e. $[\text{Fe}/\text{H}] < -4$) does it become completely shielded and starts to follow the behavior of the other elements by increasing with decreasing $[\text{Fe}/\text{H}]$. ^{32}S has another distinctive feature: $[\text{S}/\text{Fe}]$ exceeds $[\text{C}/\text{Fe}]$ at very low metallicity despite the higher initial abundance of C as compared to S in the PopIII-SNII ejecta. It turns out that Sulfur is among the main spallation products from Ni-spallation for $t_{\text{delay}} < 5$ days (i.e. $[\text{Fe}/\text{H}] \sim -4$). This produced S adds to the original S which explains why $[\text{S}/\text{Fe}]$ exceeds $[\text{C}/\text{Fe}]$ for our fiducial values. The trend of $[\text{S}/\text{Fe}]$ versus $[\text{Fe}/\text{H}]$ in extremely metal-poor stars requires further monitoring and observations before its dependence on metallicity can be confirmed (e.g. Nissen et al. 2007; Spite et al. 2011 and references therein) and put our findings to test.

3.2.5 Comparing to the average star

Figure 4 is a comparison of yields from a typical dsQN experiencing spallation in the inner and outer layers (i.e. in the $t_{\text{inner}} < t_{\text{delay}} < t_{\text{outer}}$ regime which corresponds to $-4 < [\text{Fe}/\text{H}] < -3$ in our model); we chose $t_{\text{delay}} = 6.5$ days. Our simulation results are compared to abundance pattern shared by the majority of the stars in the metallicity range $-4.0 < [\text{Fe}/\text{H}] < -3.0$ with a normal $[\text{C}/\text{Fe}]$ ratio (Cayrel et al. 2004; Spite et al. 2005; see also Figure 1 in Limongi&Chieffi 2012). As can be seen from Figure 4, both the $E_{\text{QN}} = 10$ GeV and $E_{\text{QN}} = 5$ GeV simulations are successful in reproducing the observed abundances. Note the the high abundances of Fluorine and Scandium which are spallated in the innermost layers in our model; these two rare elements are natural products of spallation (see §6.2 in Ouyed (2013)). The $E_{\text{QN}} = 5$ GeV simulations underestimate the $[\text{C}/\text{Fe}]$ and $[\text{O}/\text{Fe}]$ abundances but this is easily remedied by increasing the original carbon and oxygen content in the PopIII-SNII ejecta to reasonable amounts.

3.3 Nitrogen in our model

As shown in Ouyed (2013; see §3.3 in that paper), ^{14}N forms by spallation in the $A > 14$ layers in the PopIII-SNII ejecta. However, we find that ^{14}N can also be enhanced by the injection of protons from spallation into the C-rich and O-rich outer layers if temperatures in the PopIII-SN ejecta exceeds $\sim 1.6 \times 10^7$ K when it is hit by the QN ejecta. The carbon (and perhaps oxygen) could subsequently be processed into ^{14}N via the CN(O) cycle (Arnett 1996). For an adiabatic expansion of the preceding SN shell (i.e. $T_{\text{env.}} \propto t^{-2}$), the $T_{\text{env.}} > 1.6 \times 10^7$ K necessary condition for CN (proton capture) process to take place yields

$$t_{\text{delay}} < \sim 5 \text{ days} \frac{R_{\text{prog.,100}} T_{\text{env.,10}}^{1/2}}{v_{\text{sn,5000}}}, \quad (4)$$

where $R_{\text{prog.,100}}$ is the initial radius of the progenitor in units of $100R_{\odot}$ (R_{\odot} is the solar radius) and $T_{\text{env.,10}}$ the initial temperature of the PopIII-SNII envelope in units of 10^{10} K. For our fiducial parameters, the above translates to (see Figure 1 in Ouyed 2013)

$$\left[\frac{\text{Fe}}{\text{H}} \right] < -4. \quad (5)$$

We find that the CN(O) processing of a small percentage ($< 10\%$) of the carbon and oxygen into ^{14}N is enough to account for the

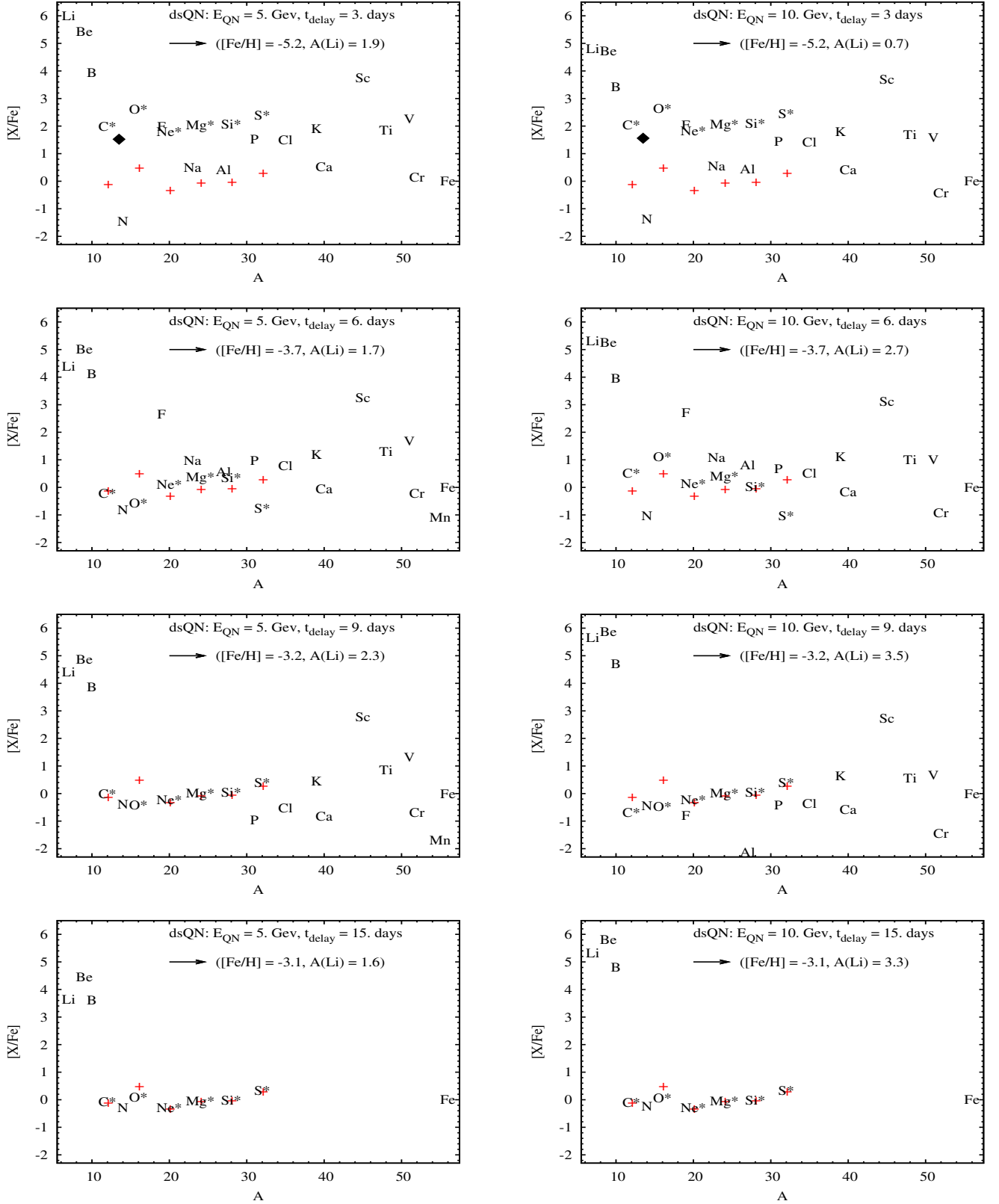


Figure 1. Relative abundances $[X/Fe]$ for spallation (sub-Fe) products versus mass number A ($7 \leq A < 56$; only stable isotopes are shown here and in other figures in this paper) for a dsQN with 5 GeV (left panels) and 10 GeV (right panels) QN neutrons. Letters show abundances from our simulations with the CN enhanced nitrogen (for short t_{delay}) shown as a filled diamond. The panels from top to bottom are for t_{delay} (days) = 3, 6, 9, 15, respectively. Also shown are the resulting $[Fe/H]$ and 7Li abundance, $A(Li)$. The plus signs represent the initial relative abundance of the original PopIII-SNII elements; these elements are identified by an asterisk (next to their names) as they evolve with t_{delay} . Their initial abundances in mass are $M_{Ni,SN} = 0.1 M_{\odot}$, $M_{S,SN} = M_{Si,SN} = M_{Mg,SN} = M_{Ne,SN} = 0.05 M_{\odot}$, $M_{O,SN} = 1.5 M_{\odot}$ and $M_{C,SN} = 0.15 M_{\odot}$. These initial abundances are the same in all of the figures in this paper unless stated otherwise. Similarly, unless stated otherwise, the mass of the cloud swept by a dsQN is set to $M_{sw} = 10^5 M_{\odot}$ in all of our simulations.

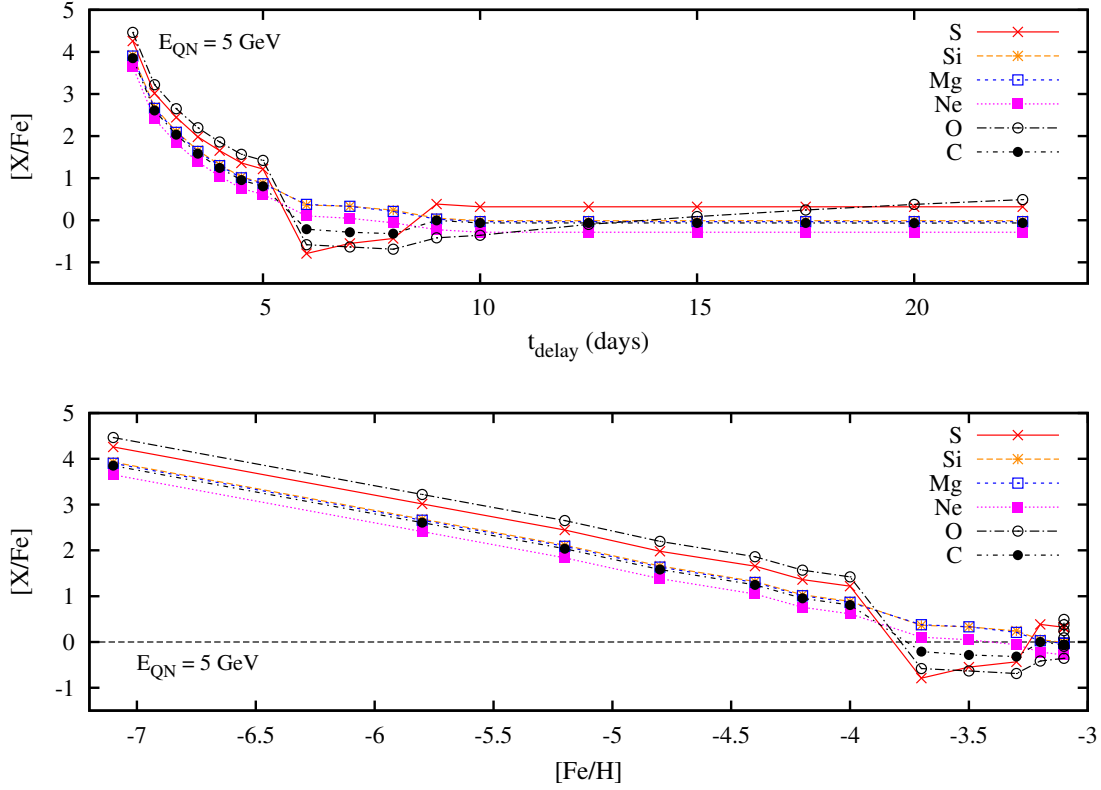


Figure 2. Relative abundances $[X/Fe]$ versus t_{delay} (top panel) and versus the corresponding $[Fe/H]$ (bottom panel) for ^{32}S , ^{28}Si , ^{24}Mg , ^{20}Ne , ^{16}O and ^{12}C with initial relative abundances $[X/Fe]_{X,\text{SN}} = 0.32, -0.01, -0.03, -0.28, 0.53, -0.09$, respectively. These elements represent the original composition of the PopIII-SNII ejecta (i.e. the target material) in our model. Here, $E_{QN} = 5 \text{ GeV}$. The horizontal dashed line in the bottom panel corresponds to $[X/Fe] = 0$.

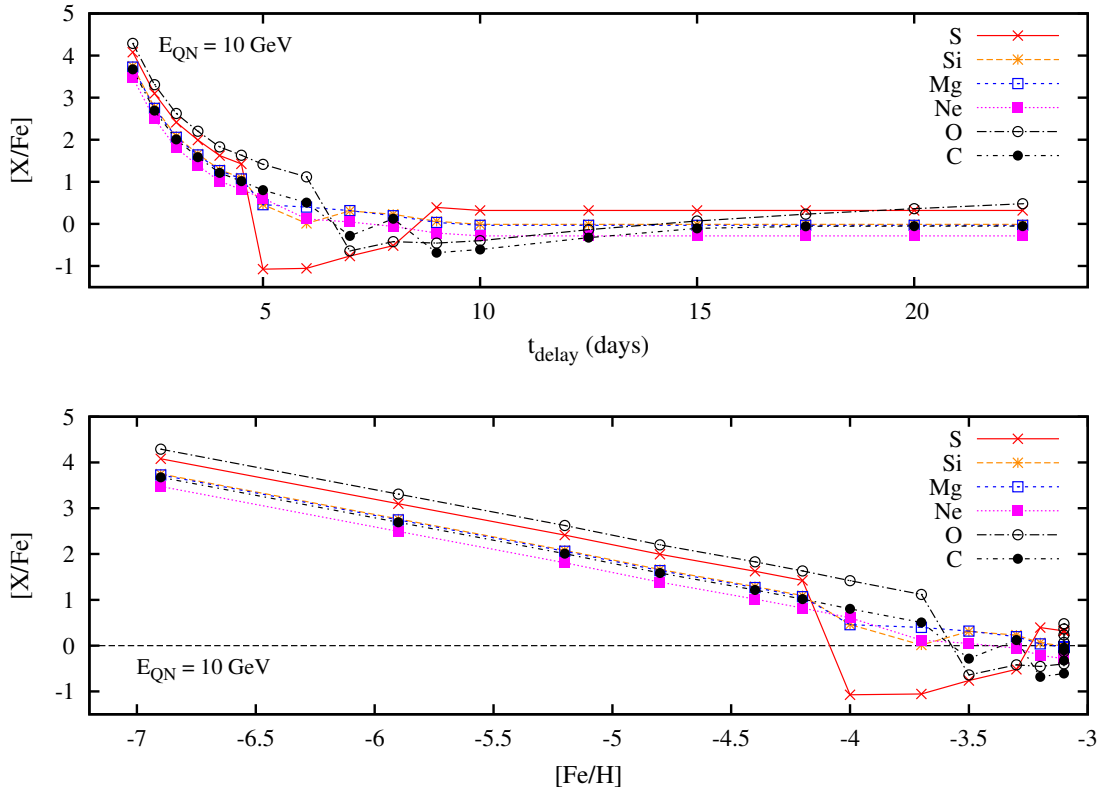


Figure 3. Same as in figure 2 but for $E_{QN} = 10 \text{ GeV}$.

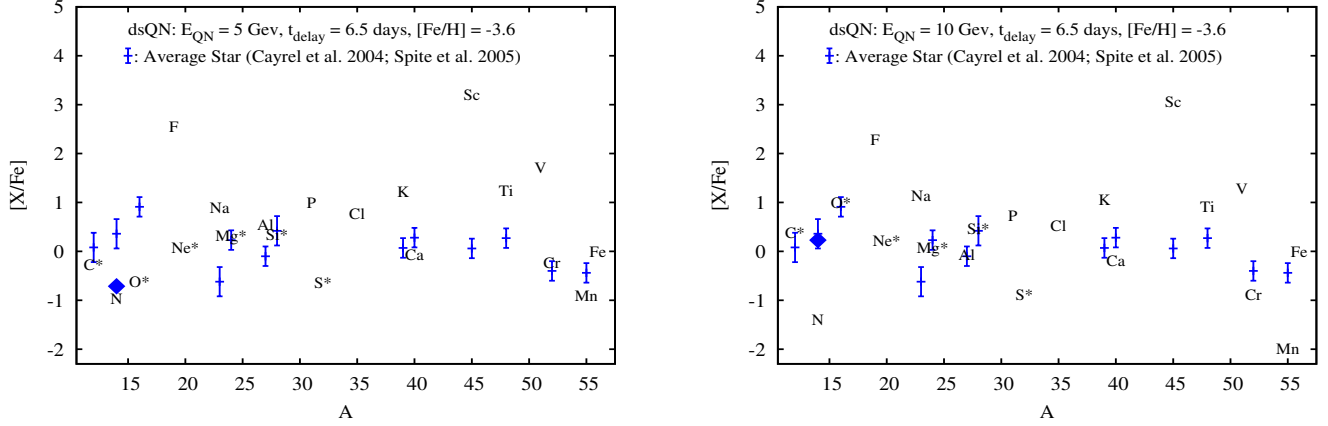


Figure 4. Relative abundances $[X/Fe]$ of sub-Fe spallation products (elements identified by their names) versus mass number A from simulations with $t_{\text{delay}} = 6.5$ days; this resulted in $[Fe/H] \approx -3.6$. The CN enhanced nitrogen is shown by the filled diamond. Measured abundances of an average halo star (Cayrel et al. 2004; Spite et al. 2005) are also shown as plus (+) signs, with corresponding uncertainties, for a comparison. Left-hand and right-hand panels are for QN neutrons with $E_{\text{QN}} = 5$ GeV and 10 GeV, respectively.

observed $[N/Fe]$ values in an average star (in Figure 4 the CN enhanced nitrogen is identified with a filled diamond). The ^{13}C abundance should also be enhanced if CN equilibrium is established in which case the $^{12}\text{C}/^{13}\text{C}$ ratios should be of the order of a few (see however Caughlan & Fowler 1972). In our model, ^{14}N production from CN cycling could occur at higher $[Fe/H]$ when taking into account envelope reheating by the QN shock (following impact on the SN ejecta). However, we caution that our model is more detailed than the standard CN cycle and would need further investigations for better estimates of ^{14}N enhancement and the expected $^{12}\text{C}/^{13}\text{C}$ values.

4 LITHIUM SYNTHESIS IN OUR MODEL

The ^7Li produced by spallation on a target A_T in the ejecta of the PopIII-SNII ejecta is given by eq.(14) in Ouyed (2013):

$$A(\text{Li}) \approx \log \eta_7^{A_T} + \log \frac{M_{A_T, \text{SN}}/1.5M_{\odot}}{M_{\text{sw}}/10^5 M_{\odot}} + 6.33, \quad (6)$$

where $\eta_7^{A_T} = M_{7\text{Li}}/M_{A_T, \text{SN}}$ is the normalized mass yields of ^7Li following spallation on target A_T with initial mass $M_{A_T, \text{SN}}$; the $1.5M_{\odot}$ is representative of our fiducial value for the oxygen content in mass in the PopIII-SNII ejecta. The final ^7Li abundance is a combination of ^7Li produced from spallation on each of the targets present in the PopIII-SNII ejecta.

Shown in Figure 5 is the ^7Li abundances resulting from spallation by $E_{\text{QN}} = 5$ GeV (left panels) and $E_{\text{QN}} = 10$ GeV (right panels) QN neutrons on a typical PopIII-SNII ejecta in our model. The top panels show $A(\text{Li})$ from simulations spanning a range in ^{56}Ni content of the PopIII-SII ejecta ($0.05M_{\odot} \leq M_{\text{Ni}, \text{SN}} \leq 0.5M_{\odot}$) and a range in t_{delay} (2 days $\leq t_{\text{delay}} \leq 24$ days). The bottom panels show the corresponding metallicity $[Fe/H]$; as explained in 3.2.1 there is a direct connection between t_{delay} and $[Fe/H]$ in our model. For $t_{\text{delay}} > 24$ days the QN neutrons traverse the PopIII-SNII ejecta with minimal interaction; i.e. no spallation occurs and the PopIII-SNII ejecta abundances would not be modified or affected (i.e. $\eta_A^{A_T} = 1$). While ^{56}Ni content was varied, the other initial abundances in mass in the PopIII-SNII were set to their fiducial values: $M_{\text{Si}, \text{SN}} = M_{\text{Mg}, \text{SN}} = M_{\text{Ne}, \text{SN}} = 0.05M_{\odot}$, $M_{\text{O}, \text{SN}} = 1.5M_{\odot}$

and $M_{\text{C}, \text{SN}} = 0.15M_{\odot}$. We adopt a $10^5 M_{\odot}$ of pristine cloud (the cradle of the Pop II low-mass stars) swept up by the SN+QN ejecta (e.g. Shigeyama&Tsujimoto 1998).

The different panels in Figure 6 (Figure 8) show the resulting $A(\text{Li})$ versus t_{delay} for each target for the $E_{\text{QN}} = 5$ GeV ($E_{\text{QN}} = 10$ GeV) simulations. The corresponding $A(\text{Li})$ versus $[Fe/H]$ is shown in Figure 7 (Figure 9). The lower right panel in Figure 6 (Figure 8) shows the combined $A(\text{Li})$ versus t_{delay} which effectively corresponds to the projection of the upper left (right) panel in Figure 5 onto the $A(\text{Li})$ - t_{delay} plane. Similarly, the lower right panel in Figure 7 (Figure 9) shows the combined $A(\text{Li})$ versus $[Fe/H]$ which effectively corresponds to the projection of the lower left (right) panel in Figure 5 onto the $A(\text{Li})$ - $[Fe/H]$ plane. One can see from these panels that ^7Li is produced in the ^{56}Ni and ^{32}S layers when $t_{\text{delay}} < t_{\text{outer}}$ and in the oxygen and carbon layers for longer delays ($t_{\text{outer}} \sim 8.3$ days is shown by the vertical dashed lines in the figures). No ^7Li is spallated in the intermediate layers (Si, Mg, Ne) and in general ^7Li is mainly produced either in the innermost layers or in the outermost CO layers. The vertical dotted lines defines the $N_{\text{mfp}, \text{C}} = \Delta R_{\text{C}}/\lambda_{\text{sp}, \text{C}} = 1$ boundary which defines a timescale above which the spallation mfp exceeds the thickness of the C-layer; i.e. no C-spallation occurs for longer time delays even if the neutrons exiting the O-layer have energies exceeding $E_{\text{sp}, \text{C}} \sim 0.42$ GeV which is above the critical value for C-spallation to ensue.

There is a gap in the ^7Li abundance (i.e. a drop in the $A(\text{Li})$ value) in the intermediate regime, $t_{\text{inner}} < t_{\text{delay}} < t_{\text{Ni}}$ (which corresponds to $-4 < [Fe/H] < -3$) since most neutrons end up being used for spallation of $A > 7$ elements in the inner layers. Thus, for Pop II low-mass stars formed from clouds swept up by dsQNe with $t_{\text{delay}} < 8.3$ days (i.e. for $[Fe/H] < -3$), the resulting ^7Li abundance would show a larger scatter mainly because in these dsQNe ^7Li is not the main spallation product and the neutrons are used up to make many other spallation products. At this point, we must note that the ^7Li abundance in dsQNe leading to $[Fe/H] < -3$ (i.e. in $t_{\text{delay}} < \sim 10$ days dsQNe) should be considered upper limits in our model. For such dsQNe, the SN ejecta is still hot ($T > 2.5 \times 10^6$ K) when it is spallated. Combined with the copious production of protons (see Tables 1 and 2), we expect most of the spallated ^7Li to be destroyed by reactions with the protons or at least become reduced (see §5 in Ouyed 2013).

4.1 The high-scatter, $A(\text{Li}) \sim 2.2$, plateau

Two “plateaus” can be seen in the top right panel in Figure 5 (i.e. for the $E_{\text{QN}} = 10$ GeV simulation). One resulting from O-spallation with $1.8 < A(\text{Li}) < 2.5$ and a second one from C-spallation with $2.5 < A(\text{Li}) < 3.5$. These two plateaus can also be seen in panels labeled “C-Target” and “O-Target” in Figures 6, 7, 8, 9. Both occur for $t_{\text{delay}} > t_{\text{outer}} \sim 8.3$ days which means that the QN neutrons proceed directly into the outer layers with minimal interaction with the Ni, S, Si, Mg and Ne layers. Spallation in the O-layer leads to smaller ${}^7\text{Li}$ abundance and more scatter in the ${}^7\text{Li}$ plateau since the neutrons spallate more products than in the case of spallation in the C-layer.

We first focus on the $A(\text{Li}) \sim 2.2$ plateau uncovered in our simulations (the $A(\text{Li}) = 2.2$ value is indicated by the horizontal planes in Figure 5 and by the horizontal lines in Figures 6, 7, 8, 9). This plateau is populated by ${}^7\text{Li}$ spallated from oxygen for dsQNe with $t_{\text{delay}} > 8.3$ days. As can be seen from Figure 5, while the $E_{\text{QN}} = 5$ GeV simulations yield $A(\text{Li})$ approaching the 2.2 value from the lower bound, barely exceeding it, the $E_{\text{QN}} = 10$ GeV simulations yield ${}^7\text{Li}$ abundances oscillating around $A(\text{Li}) \sim 2.2$ (with $1.8 < A(\text{Li}) < 2.5$). To understand this interesting finding from our simulations we first note that in each sub-layer i (i.e. for each mfp, $\lambda_{\text{sp},\text{O}}$) of the O-layer, the distribution of the atomic weights of the spallation products is close to a normal distribution peaking at $A_{\text{peak},i} \sim A_{\text{T}} - \zeta_{\text{av},i}$ where $\zeta_{\text{av},i}$ is the average multiplicity for sub-layer i (see Table 2). For each sub-layer the corresponding amount in mass of spallated ${}^7\text{Li}$ can be estimated from the corresponding distribution.

Since the highest ζ_{av} is induced in the first sub-layer this leads to a peak spallation product ($A_{\text{peak}} = 16 - \zeta_{\text{av}}$) closest to ${}^7\text{Li}$. Subsequent sub-layers would yield peak spallation products getting closer to the target’s A_{T} (here $A_{\text{T}} = 16$) thus reducing the ${}^7\text{Li}$ contribution to the overall distribution of the spallated elements and thus a reduction in the final amount of ${}^7\text{Li}$ spallated. However, for subsequent sub-layers the multiplicity is higher and more neutrons+protons induce spallation. The final abundances of the spallation products is a combination of these distributions (see e.g. Figure 1 in Ouyed et al. 2011) which yields $M_{\text{Li}} \sim \alpha_7 \zeta_{\text{net}} M_{\text{QN}} \equiv \beta_7 M_{\text{QN}}$ where $\beta_7 = \alpha_7 \zeta_{\text{net}}$. Since the ${}^7\text{Li}$ contribution given by the distributions is roughly $\alpha_7 \sim 0.01$ (of the order of $\sim 1\%$) and $\zeta_{\text{net}} \sim 10$ (see e.g. Table 2) this yields $\beta_7 \sim 0.1$. The corresponding ${}^7\text{Li}$ abundance $A(\text{Li}) = \log N_{7\text{Li}}/N_{\text{H}} + 12$ is then roughly estimated to be

$$A(\text{Li}) \sim 2.15 + \log \left(\beta_{7,0.1} \frac{M_{\text{QN}}/10^{-3} M_{\odot}}{M_{\text{sw}}/10^5 M_{\odot}} \right), \quad (7)$$

where we made use of $N_{7\text{Li}} = M_{7\text{Li}}/7m_{\text{H}}$ and $N_{\text{H}} = M_{\text{sw}}/m_{\text{H}}$. The amount of ${}^7\text{Li}$ spallated is roughly equivalent to a normalized mass yield $\eta_7^{16} \sim 6.7 \times 10^{-5}$ or $\log \eta_7^{16} \sim -4.17$ for our fiducial values; i.e. $A(\text{Li}) \sim 2.15$ from using eq.(6).

The weak dependence of the multiplicity on energy leads to similar distributions of spallation products in the oxygen layer for the range in E_{QN} expected in QNe explosions. This translates to similar ζ_{net} and α_7 (i.e. β_7) values which explains why the $E_{\text{QN}} = 5$ GeV also hovers around the same $A(\text{Li})$ value and effectively implies that $A(\text{Li})$ is mainly dependent on M_{QN} and M_{sw} . In fact by scaling M_{sw} with M_{QN} (i.e. with the kinetic energy, $E_{\text{QN}}^{\text{KE}}$, of the QN ejecta) we always recover an $A(\text{Li})$ close to Spite values when $t_{\text{delay}} > t_{\text{outer}}$; i.e. when spallation occurs mainly in the outer oxygen and carbon layers as shown in §4.2 below.

4.1.1 The C-spallated ${}^7\text{Li}$ plateau

When $\Delta R_{\text{C}} < \lambda_{\text{sp},\text{C}}$, even if enough neutrons with energy above $E_{\text{sp},\text{C}} \sim 0.42$ GeV make it past the O-layer, they will not interact with the overlaying carbon and there will be no spallated ${}^7\text{Li}$ and the corresponding plateau would disappear. From eq. (1), the $N_{\text{mfp},\text{C}} > 1$ condition (i.e. $\Delta R_{\text{C}} > \lambda_{\text{sp},\text{C}}$) yields $t_{\text{delay}} < \sim 13$ days $\times (M_{\text{C},\text{SN}}/0.15 M_{\odot})^{1/2}$ for our fiducial values. This means that spallation in the C-layer would occur mainly when $t_{\text{outer}} \sim 8$ days $< t_{\text{delay}} < 13$ days which is a narrow window. On the other hand, if we increase the carbon content in the PopIII-SNII ejecta as to make $\Delta R_{\text{C}} > \lambda_{\text{sp},\text{C}}$ then spallation would ensue. Figure 10 shows the two plateaus again for $E_{\text{QN}} = 10$ GeV but for much higher carbon content than our fiducial values (here $M_{\text{C},\text{SN}} = M_{\text{O},\text{SN}} = 1.5 M_{\odot}$). As can be seen in the figure, although the plateau from O-spallation is close to the Spite value, it is clearly dwarfed by the ${}^7\text{Li}$ produced in carbon layer. For $M_{\text{C},\text{SN}} = 1.5 M_{\odot}$, the $\Delta R_{\text{C}} < \lambda_{\text{sp},\text{C}}$ regime occurs when $t_{\text{delay}} > 30$ days beyond which the C-spallated ${}^7\text{Li}$ plateau disappears. We find that in PopIII-SNII with high carbon content, and in particular those with $E_{\text{QN}} \geq 10$ GeV, the ${}^7\text{Li}$ plateau from C-spallation is dominant and far exceeds the Spite value. Another possibility would consist of reducing oxygen content in the PopIII-SNII ejecta so that the primary (i.e. QN) neutrons experience only a very few interactions (mfps) in the oxygen layer before making their way towards the C-layer. This is the least likely scenario since it seems that oxygen is produced in much larger quantity than carbon in PopIII-SNII ejecta (e.g. Umeda&Nomoto 2002).

On average, spallated neutrons in the $E_{\text{QN}} = 5$ GeV case acquire lower energies than the $E_{\text{QN}} = 10$ GeV case. Thus, there is no substantial amounts of ${}^7\text{Li}$ spallated in the C-layer since fewer > 0.42 GeV neutrons manage to make past the O-layer. The resulting plateau is very scattered and remains below Spite values; see the panels labeled “C-Target” in Figures 6 and 7.

4.2 A low-scatter, $A(\text{Li}) \sim 2.2$, plateau

If we associate high E_{QN} dsQNe with short time delays and low E_{QN} dsQNe with relatively longer delays (> 15 days), a low-scatter plateau results as shown in Figure 11. The top panel shows abundances from simulations with $E_{\text{QN}} = 10$ GeV and $M_{\text{sw}} = 10^5 M_{\odot}$ with 5 days $< t_{\text{delay}} < 15$ days. The middle panel shows results from an $E_{\text{QN}} = 5$ GeV simulation with $M_{\text{sw}} = 10^{4.5} M_{\odot}$ and for 15 days $< t_{\text{delay}} < 30$ days. The combined ${}^7\text{Li}$ abundance from these simulations leads to a plateau with features reminiscent of the observed one. To extend the plateau to higher [Fe/H] values we had to include simulations where the mass of the pristine cloud swept up by the dsQN is lower than the fiducial value of $10^5 M_{\odot}$. For example, the $M_{\text{sw}} = 10^{4.5} M_{\odot}$ simulations effectively shift the plateau to the right in Figures 7 and 9 by yielding [Fe/H] values close to ~ -2 (see eq. 3). However, a decrease in M_{sw} increases the $A(\text{Li})$ value (see eq. 6) which is remedied by a decrease in E_{QN} which decreased the amounts of spallated ${}^7\text{Li}$ accordingly. The high $A(\text{Li}) \sim 3.5$ values in the top panel correspond to abundances from C-spallation. However, the thinnest plateaus result from simulations which minimize spallation in the C-layer. This meant setting $M_{\text{C},\text{SN}} < 0.1 M_{\odot}$ for our fiducial values, or in general by taking $M_{\text{C},\text{SN}} < M_{\text{O},\text{SN}}/10$.

While more sophisticated calculations may be required to further constrain the parameters, the QN model naturally explains this dichotomy: In general, the reduced mass-loss in Pop III stars means that the more massive progenitors could in principle end up with the more massive cores at explosion and should thus lead to heavier NSs. Or, if fallback is greater from the more massive QN pro-

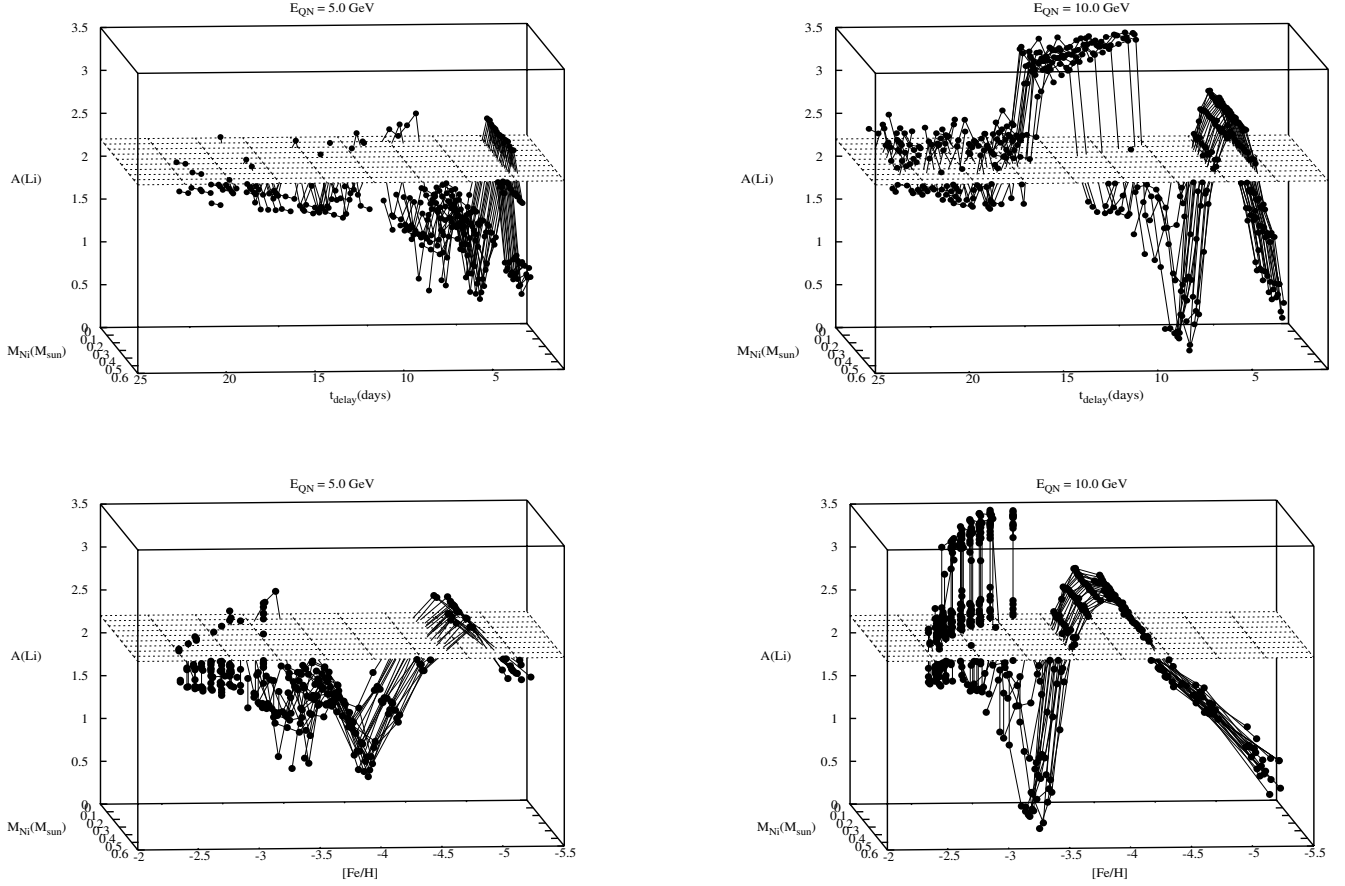


Figure 5. Top panels: $A(\text{Li})$ versus time delay ($2 \text{ days} \leq t_{\text{delay}} \leq 30 \text{ days}$) and PopIII-SNII initial ^{56}Ni mass ($0.1 M_{\odot} \leq M_{\text{Ni,SN}} \leq 0.5 M_{\odot}$). Bottom panels: The corresponding $A(\text{Li})$ versus $[\text{Fe}/\text{H}]$ ($-7.5 < [\text{Fe}/\text{H}] < -2.5$; see 3.2.1). Left-hand and right-hand panels are for $E_{\text{QN}} = 5 \text{ GeV}$ and 10 GeV , respectively. The horizontal plane corresponds to $A(\text{Li}) = 2.2$.

genitors (i.e. those closer to the black hole limit which we set here to be $40 M_{\odot}$), this should also translate to the formation of a more massive compact remnant (i.e. a parent NS with higher core density). These heavier NSs should undergo a QN explosion on shorter time delays as found by Staff et al. (2006). The core-collapse of the massive progenitors followed by the QN explosion of the massive NS would likely lead to a more energetic SN+QN ejecta which should sweep up more pristine material (i.e. M_{sw} should be higher in these dsQNe; e.g. Shigeyama&Tsujimoto 1998). Naturally, the shorter time delay (i.e. the lower $[\text{Fe}/\text{H}]$) dsQNe would lead to a higher scatter in the plateau, and its eventual meltdown for the shortest delay dsQNe, since ^7Li will be produced in the inner layers from multiple targets. In this picture, low-mass Pop II stars in the Spite plateau would have originated from pristine clouds swept up by dsQNe with progenitors in the lower end of the mass range, $20 M_{\odot} < M_{\text{prog.}} < 40 M_{\odot}$, with reduced fallback. As discussed later (see §5), dsQNe with short delays should be the rarest among dsQNe. The implication is that the resulting Pop II stars (those with very low $[\text{Fe}/\text{H}]$ and high $A(\text{Li})$ scatter according to our model) would be the rarest among very metal-poor stars.

4.3 Discussion

We now discuss some implications of our findings to Lithium in the Universe:

- **The BBN component:** In this work and in Ouyed (2013), we have neglected the BBN contribution in the cloud swept up by the SN+QN ejecta and considered only $A(\text{Li})$ from dsQN spallation on PopIII-SNII ejecta. Among plausible scenarii that could lead to the destruction of the BBN component in pristine clouds, before they get swept up by the combined SN+QN ejecta, are:

- (i) The QN provides copious amount of neutrons with some of them freely streaming ahead of the combined SN+QN ejecta. These free QN neutrons could destroy the BBN ^7Li (e.g., see Albornoz Vásquez et al. 2012 and references therein for relevant nuclear reactions). This might contribute to the destruction of the surrounding BBN ^7Li before material is swept up by the SN+QN ejecta – this remains to be confirmed;

- (ii) A massive astration of ^7Li by processing in Pop III stars as suggested by Piau et al. (2006). This model provides a natural connection to ours since it appeals to Pop III stars in the $10 M_{\odot}$ - $40 M_{\odot}$ mass range; the favored QN progenitor mass range. Thus, adopting the Piau et al. (2006) hypothesis, one could then envision a scenario in which the BBN ^7Li is processed and destroyed by the Pop

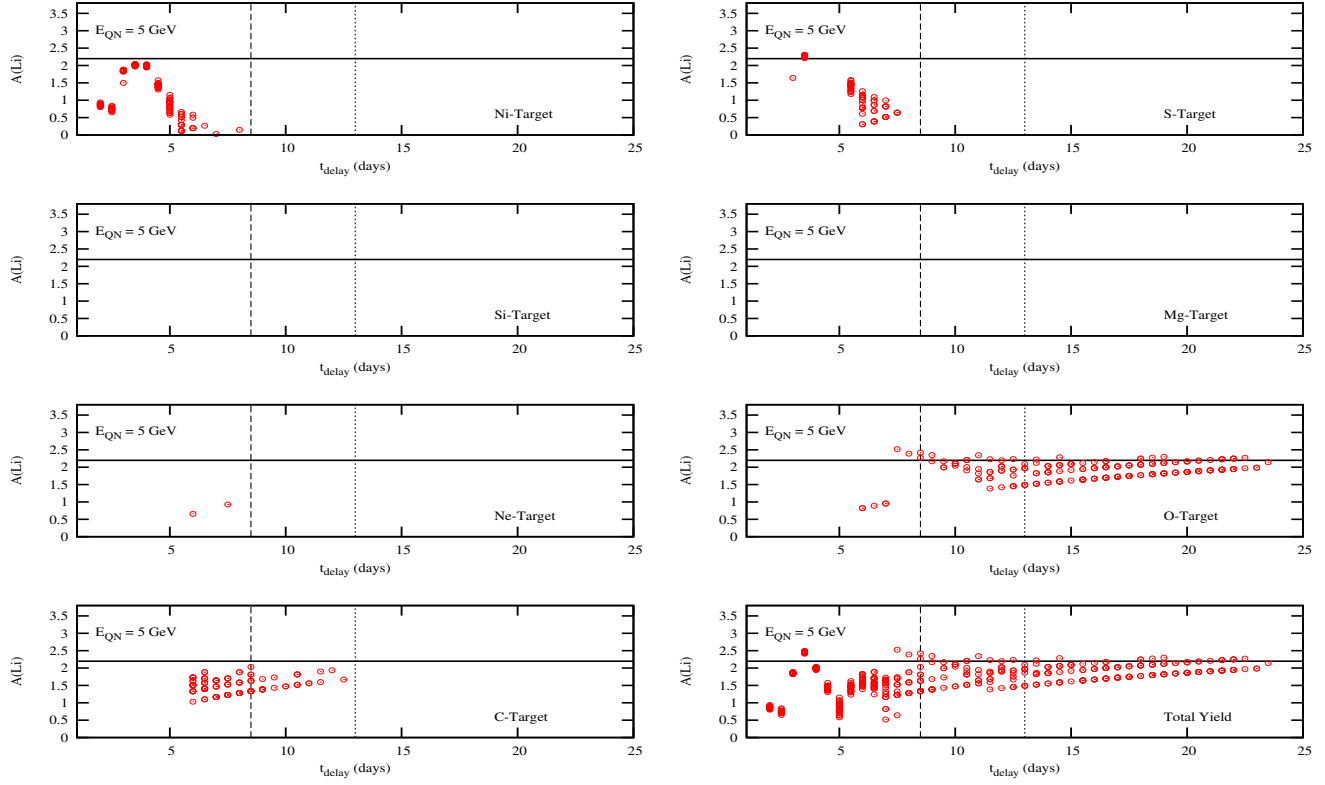


Figure 6. The open circles show $A(\text{Li})$ versus t_{delay} per spallation target (Ni, S, Si, Mg, Ne, O and C) for the simulations shown in the left panels in figure 5 (i.e. for $E_{\text{QN}} = 5$ GeV). The "Total Yield" panel shows $A(\text{Li})$ from all targets combined. The Horizontal lines corresponds to $A(\text{Li}) = 2.2$. The vertical dashed line shows $t_{\text{outer}} \sim 8.3$ days while the dotted vertical line is at 13 days which defines the $\Delta R_C = \lambda_{\text{sp},C}$ limit (i.e. $N_{\text{mfp},C} = 1$) above which no spallation occurs in the C layer.

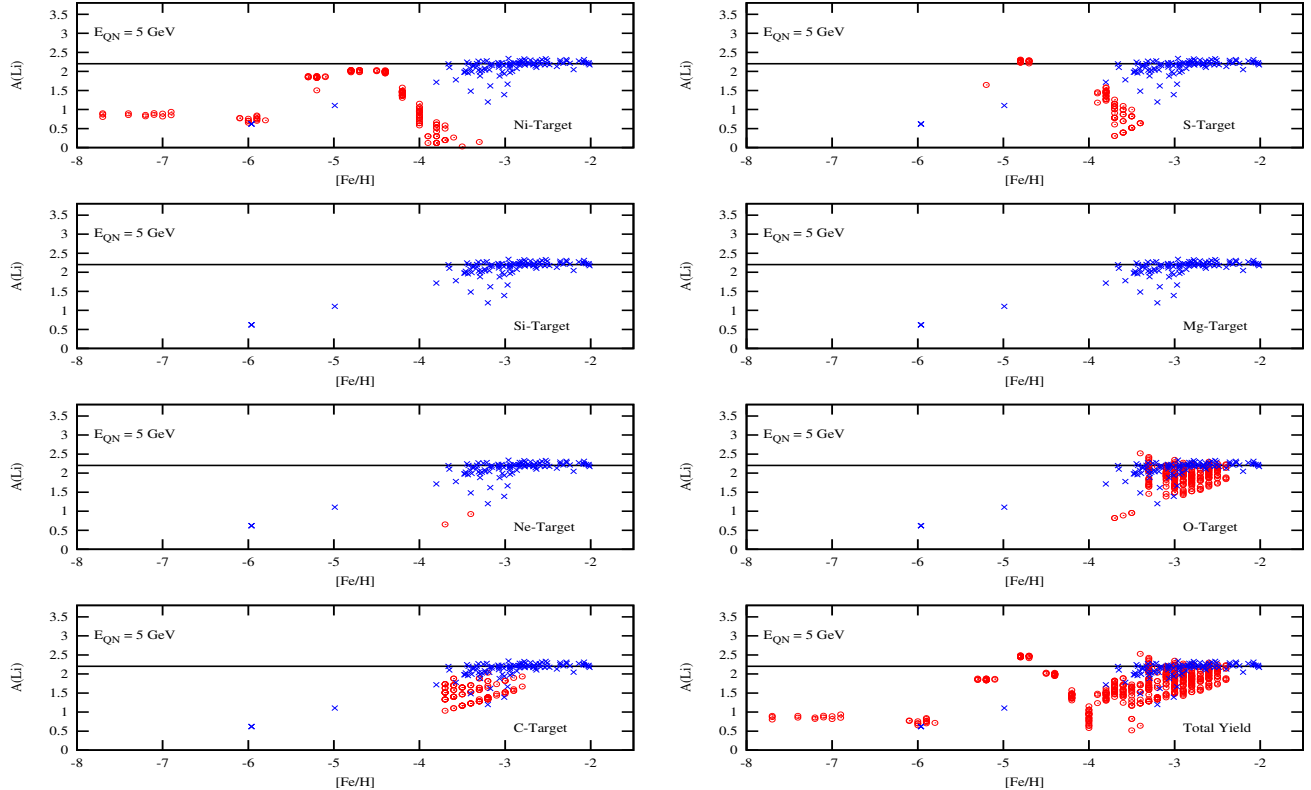


Figure 7. The open circles show $A(\text{Li})$ versus $[\text{Fe}/\text{H}]$ per spallation target (Ni, S, Si, Mg, Ne, O and C) for the simulations shown in the left panels in figure 5 (i.e. for $E_{\text{QN}} = 5$ GeV). The crosses are measured ${}^7\text{Li}$ abundances in halo and turn-off stars from Sbordone et al. (2012; see their figure 1 for references).

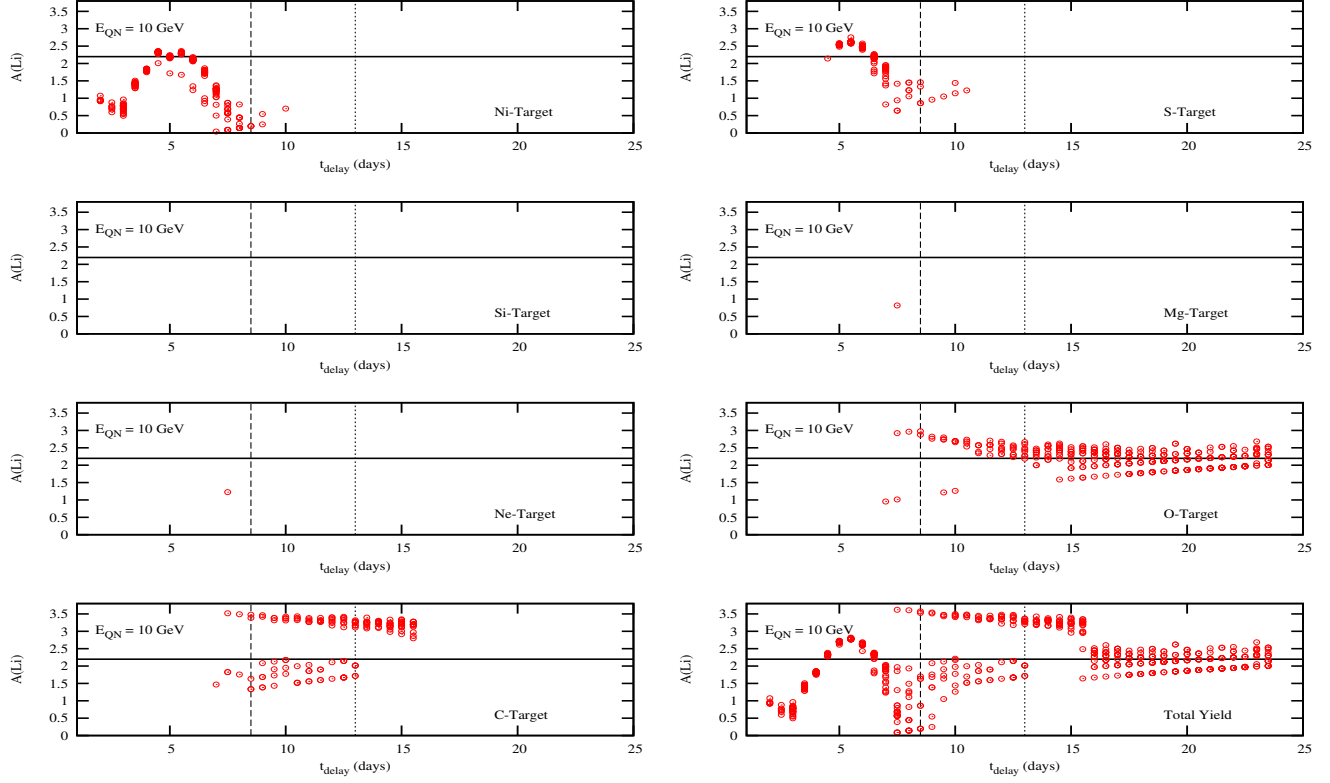


Figure 8. Same as in figure 6 but for the $E_{\text{QN}} = 10$ GeV simulations.

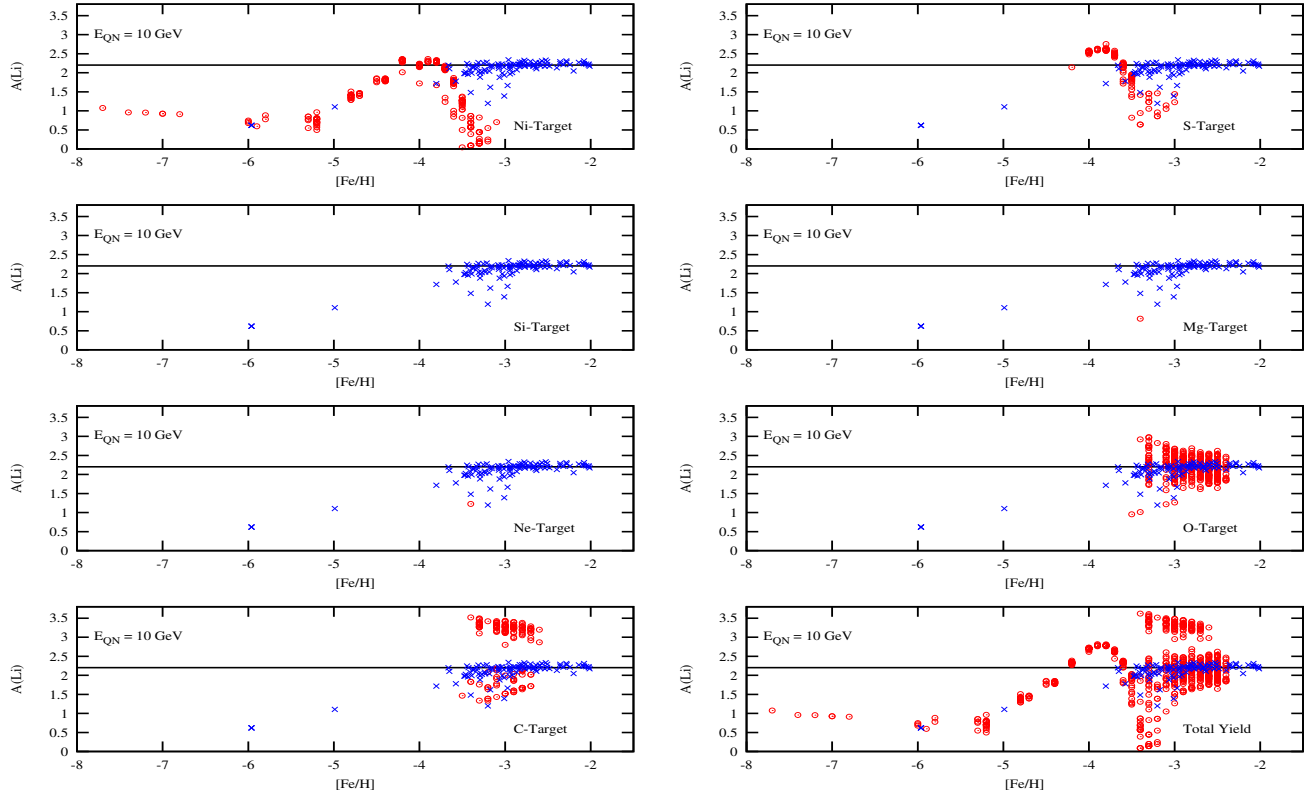


Figure 9. Same as in figure 7 but for the $E_{\text{QN}} = 10$ GeV simulations.

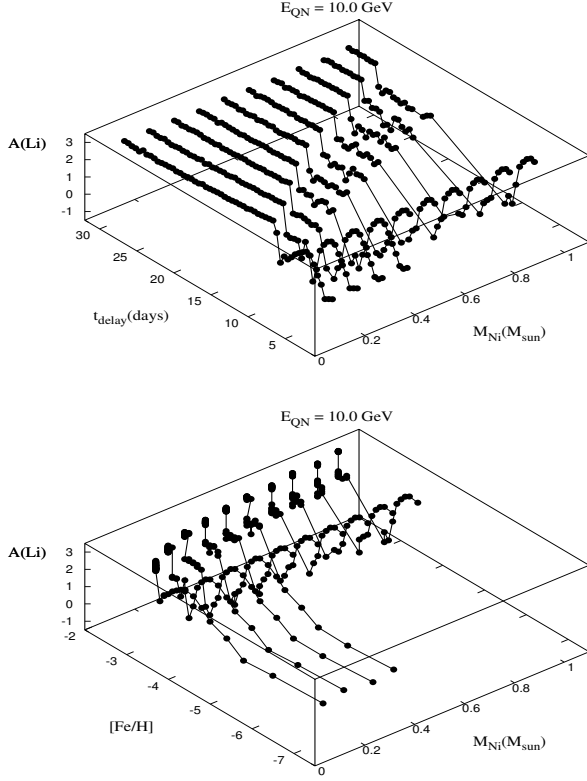


Figure 10. Same as in figure 5 but for $M_{C,SN} = M_{O,SN} = 1.5M_{\odot}$.

III star before it undergoes a PopIII-SNII explosion and the subsequent QN event. In this scenario, the issue of overproduction of CNO elements plaguing the Piau et al. (2006) hypothesis is alleviated since in our scenario these would be reduced by spallation. The pristine material/cloud swept up would then carry the imprint of ${}^7\text{Li}$ resulting from spallation of PopIII-SNII ejecta by dsQNe without the overproduction of CNO elements;

(iii) If it turns out that neither of these scenarios are satisfactory, we might envisage the bold but very unlikely proposition that ${}^7\text{Li}$ might not have been processed during BBN and is rather a relic of primordial dsQNe spallation.

• **Super-Li rich candidates:** A few super-Li rich stars have been reported in the literature exceeding the BBN value (e.g. the $A(\text{Li}) = 2.87$ star in the globular cluster M4; Monaco et al. 2012). Other stars far exceed the meteoritic values of $A(\text{Li}) = 3.25$ (Deliyannis et al. 2002; Koch et al. 2012; Adamów et al. 2012). Standard enhancement scenarios including planetary ingestion, Hypernovae, outward radiative acceleration of ${}^7\text{Li}$ from deeper regions in the stars, and binary transfer face challenges in explaining such extreme levels of Li-enhancement (e.g. Monaco et al. 2012; Koch et al. 2012).

In our model, such high $A(\text{Li})$ values result from spallation in the C layer. C-spallation would occur for a narrow window of time delay ($8.3 \text{ days} < t_{\text{delay}} < 13 \text{ days}$ for our fiducial values) and only if enough $> 0.42 \text{ GeV}$ neutrons make it past the O-layer; i.e. mainly in dsQNe with $E_{\text{QN}} \geq 10 \text{ GeV}$ and with $M_{C,SN} > 0.1M_{O,SN}$ (see discussion in §4.1). These stringent constraints suggest that super-Li candidates (i.e. Pop II low-mass stars with ${}^7\text{Li}$ spallated in the C-layer in our model) should be relatively rare compared to normal (i.e. with $A(\text{Li}) \sim 2.2$ from O-spallation) candidates.

• **Interstellar ${}^7\text{Li}$ abundance:** Howk et al. (2012) reported

measurements of interstellar ${}^7\text{Li}$ abundance of the Small Magellanic Cloud with values nearly equal to the BBN predictions. This suggests that contributions of galactic chemical evolution can be neglected in this case. We suggest instead that the measured value may be a signature of a gas swept up by a dsQN with important C-spallation (see discussion above). Interestingly the ${}^6\text{Li}/{}^7\text{Li} = 0.13$ measured by Howk et al. (2012) is very close to the value predicted by Ouyed (2013; see §5.3 and Fig. 8 in that paper). The high ${}^6\text{Li}/{}^7\text{Li}$ values are expected in our model since ${}^6\text{Li}$ and ${}^7\text{Li}$ would be produced with nearly equal proportions from spallation.

5 DISCUSSION AND PREDICTIONS

Below we discuss some implications of our model to the early universe followed by some specific predictions:

• **Formation of Pop II low-mass stars:** There are two models for the transition from Pop III to Pop II discussed in the literature: (i) Atomic fine-structure line cooling (Bromm & Loeb 2003). In this model, low-mass star formation can occur in gas that is enriched beyond the critical abundances of $[\text{C}/\text{H}]_{\text{crit}} \sim -3.5 \pm 0.1$ dex and $[\text{O}/\text{H}]_{\text{crit}} \sim -3 \pm 0.2$ dex (or $Z > Z_{\text{cr.}} \sim 10^{-3.5} Z_{\odot}$); (ii) Dust-induced fragmentation (e.g. Schneider et al. 2006a). The dust-cooling model predicts critical metallicity, Z , smaller by a factor of 10-100 than those predicted in line cooling models.

The discovery of SDSS J102915+172927 (Caffau et al. 2011), an ultra metal-poor (UMP) star with $[\text{Fe}/\text{H}] \sim -5$ (and with no excess of carbon) born from a cloud with $Z < Z_{\text{cr.}}$, challenges the line cooling model (see also Klessen et al. 2012) and seems to hint at a dust-induced fragmentation. However, it has been argued that dust production in very metal-poor gas is too inefficient (e.g. Silvia et al. 2010; see however Nozawa et al. 2012) in which case one should consider fragmentation at high densities as another plausible mechanism to form low-mass stars in the pristine universe (e.g. Greif et al. 2011 and references therein). In our model, Fe-poor does not translate to Z-poor since in short delay dsQNe the outer CO-rich layers should be preserved. The swept up cloud will be Fe-poor but not necessarily Z-poor. One can also have the situation where most of the PopIII-SNII C and O is spallated without destruction of the innermost layers. Furthermore, the extremely dense relativistic QN ejecta should provide high enough compression to drive the needed fragmentation in the pristine cloud swept-up by the dsQN. The cloud could in principle fragment into dense cores whose masses should be comparable to the Jeans masses and collapse to form low-mass stars that can survive to the present (Machida et al. (2005).

Figure 12 compares relative abundances of stable isotopes in a pristine cloud swept up by a $t_{\text{delay}} = 3.5 \text{ days}$ dsQN to measured values in SDSS J102915+172927. Both the $E_{\text{QN}} = 5 \text{ GeV}$ and the $E_{\text{QN}} = 10 \text{ GeV}$ simulations give very encouraging fits to measured abundances although our model overproduces ${}^{48}\text{Ti}$. As noted earlier, large abundances of Fluorine and Scandium are expected in our model since these rare nuclides are a natural outcome of spallation processes (see §6.2 in Ouyed 2013). The ${}^7\text{Li}$ shown are upper limits in our model since as we have noted, for $t_{\text{delay}} < \sim 10 \text{ days}$ (i.e. for $[\text{Fe}/\text{H}] < -3$), the PopIII-SNII envelope temperature exceeds $2.5 \times 10^6 \text{ K}$ when spallation occurs which should reduce the final abundance of the spallated ${}^7\text{Li}$.

• **The primordial, Pop III, IMF:** Our model requires no modification to the primordial IMF (the very massive Pop III found in simulations; e.g. Wise&Abel 2007) and does not contradict observations that hint at contamination of Pop II star-forming clouds by the explosions of $10M_{\odot}$ - $50M_{\odot}$ progenitors (e.g. Umeda&Nomoto

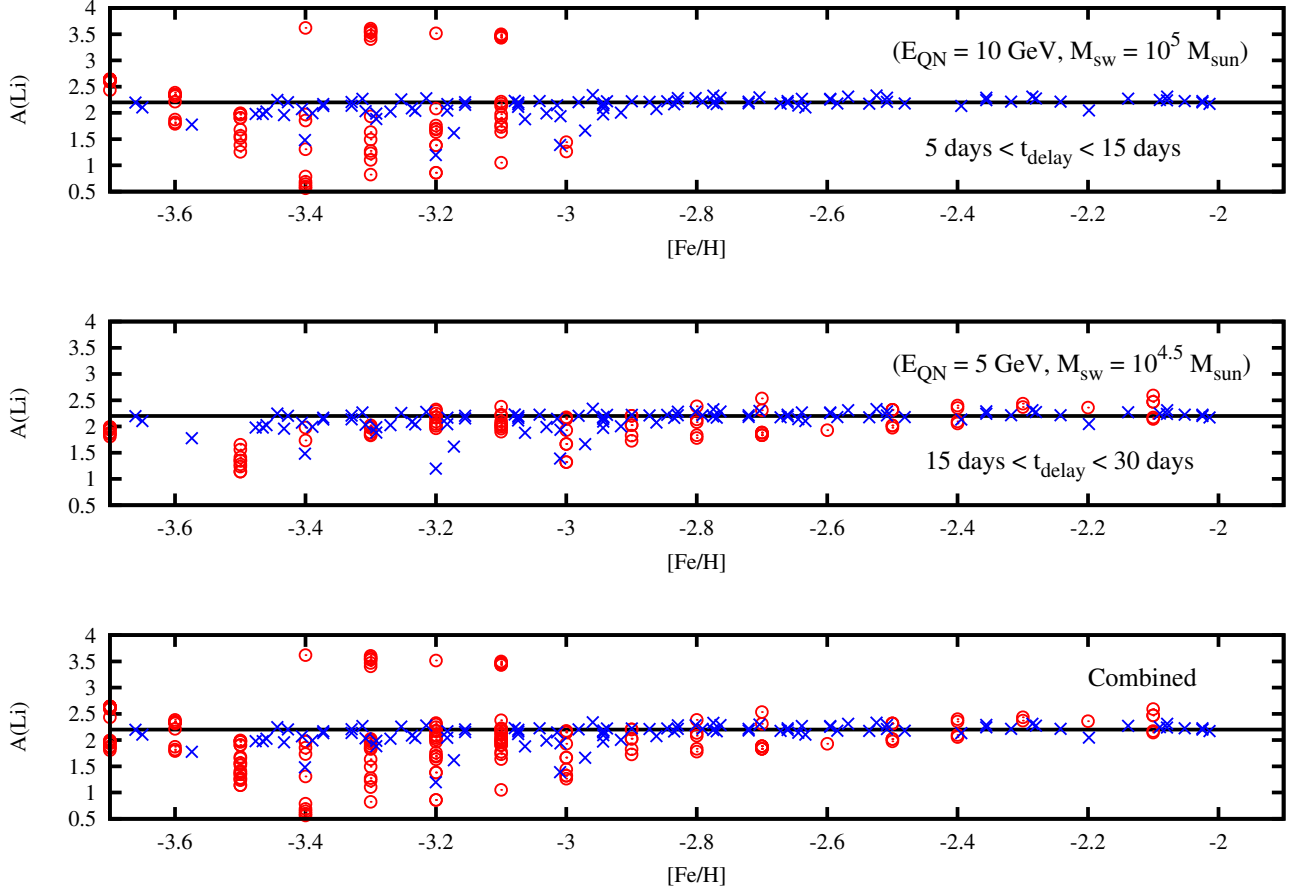


Figure 11. Top panel: $A(\text{Li})$ versus $[\text{Fe}/\text{H}]$ for simulations with $E_{\text{QN}} = 10 \text{ GeV}$, $M_{\text{sw}} = 10^5 M_{\odot}$ and for $5 \text{ days} < t_{\text{delay}} < 15 \text{ days}$. Middle panel: $A(\text{Li})$ versus $[\text{Fe}/\text{H}]$ for simulations with $E_{\text{QN}} = 5 \text{ GeV}$, $M_{\text{sw}} = 10^{4.5} M_{\odot}$ and for $15 \text{ days} < t_{\text{delay}} < 30 \text{ days}$. Bottom panel: $A(\text{Li})$ versus $[\text{Fe}/\text{H}]$ resulting from all simulations for a range in ^{56}Ni content, $0.05 M_{\odot} \leq M_{\text{Ni,SN}} \leq 0.5 M_{\odot}$. The crosses are measured ^7Li abundances in halo stars and turn-off stars as described in Sbordone et al. (2012; see their figure 1 for the sources of the data). The Horizontal line corresponds to $A(\text{Li}) \sim 2.2$.

2005; Tumlinson et al. 2004). In a heavy Pop III IMF, stars with $20 M_{\odot}$ – $40 M_{\odot}$ would lead to dsQNe. Thus our model might help reconcile the Pop III simulations and the observations of Pop II low-mass stars if the latter formed from pristine clouds swept-up by primordial dsQNe as described in this work (see §6.3 in Ouyed 2013 for more discussion and relevant references).

- **The statistics:** In a heavy Pop III IMF (e.g. see discussion in Larson 1998; see also Schneider et al. 2006b and references therein), dsQNe progenitors would contribute a small percentage of the population. Thus, according to our model, the statistics of the resulting low-mass Pop II stars in the galactic halo may be a reflection of the IMF of Pop III stars (specifically the lower mass end of the distribution). Interestingly, the statistics of the known old, $[\text{Fe}/\text{H}] < -2$ stars are intrinsically rare in the Galaxy and represent only a small percentage of the total stellar mass (see Table 3 in Beers&Christlieb 2005).

Furthermore, in the QN model, the more massive the parent neutron star (to be experiencing a QN explosion), the more likely it will reach deconfinement in short time delays (Staff et al. 2006). As we have mentioned earlier, if fallback or the size of the collapsing core increases with the QN progenitor’s mass, then these should lead to heavier NSs which are more likely to undergo a QN transition on shorter time delays. This means that short t_{delay} dsQNe should

be the rarest in a heavy Pop III IMF peaking below $\sim 40 M_{\odot}$. In other words, the lower the $[\text{Fe}/\text{H}]$ (i.e. the shorter the t_{delay}) the smaller the statistics of the ensuing Pop II stars. In this picture, Hyper-Metal Poor (HMP) stars (with $[\text{Fe}/\text{H}] < -5$ in the terminology of Beers&Christlieb 2005) would have originated in pristine clouds swept up by dsQNe from progenitors on the high end in the $20 M_{\odot} < M_{\text{prog.}} < 40 M_{\odot}$ mass range. However, this conclusion relies heavily on the exact shape of the Pop III IMF which remains to be confirmed.

- **Origin of HMP stars:** We focus here on two known HMP stars, HE0107-5240 ($[\text{Fe}/\text{H}] = -5.54$; Christlieb et al. 2002) and HE1327-2326 ($[\text{Fe}/\text{H}] = -5.76$; Frebel et al. 2008). These two stars have extremely high enhancements of the light elements C, N, and O relative to Fe. Figure 13 show a comparison of the peculiar chemical composition of HE 0107–5240 and HE 1327–2326 to abundances from dsQNe with for $t_{\text{delay}} = 2.8 \text{ days}$ and $t_{\text{delay}} = 2.6 \text{ days}$, respectively. The measured relative abundances of elements, $[\text{X}/\text{Fe}]$, in these sources we take from Norris et al. (2013; see their Table 4). In our model, HMPs would correspond to the scenario where substantial interaction occurs in the inner layer either using up the majority of the QN neutrons or reducing their energy below the critical value for O- and C-spallation to ensue (see §3 in Ouyed 2013). The shielding (from spallation by the QN neutrons)

of the outer CO layers combined with the substantial destruction of the ^{56}Ni layer explains the large $[C/Fe]$ and $[O/Fe]$ in these objects (see Figures 1, 2 and 3). We find a good fit to measured abundances except for ^{48}Ti which is overproduced in our model. There is a strong apparent depletion of lithium, ($A(\text{Li}) < 1.5$) in these two HMP stars. A strong lithium depletion in the atmosphere of HE1327-2326 is unlikely given its mass and temperature $T_{\text{eff}} \sim 6000$ K. The more massive HE0107-5240 may have depleted its own ^7Li but it is hard to imagine a process that would practically bring its abundance much below the plateau. Our model leads to the right levels of ^7Li abundances although the ^7Li abundance from our simulations should be considered upper limits since $[\text{Fe}/\text{H}] < -3$ for HMPs (see §4.1).

There have been investigations on the origins of the HMP stars. It has been argued that the binary mass transfer hypothesis provides best fits to the overall abundances of these stars (Suda et al. 2004). This hypothesis remains to be confirmed by the discovery of radial velocity variations in HMP stars. Furthermore, this hypothesis implies that the stellar IMF at $Z < 10^{-5}Z_{\odot}$ was biased towards intermediate mass stars (Tumlinson 2007). The large C enhancement with respect to Fe in HMPs stars we argue, might not be an indication of binarity (e.g. Suda et al. 2004) but rather a direct consequence of important ^{56}Ni (and thus Fe) destruction and a preservation of the carbon in the PopIII-SNII ejecta. In the binary accretion scenario, high level of C should be accompanied by high levels of s-process which is not always observed (e.g. Cohen et al. 2006). In the dsQN model, slow neutrons capture processes and the resulting s-process products become important in dsQNe with t_{delay} leading to HMP stars (see §4 in Ouyed 2013 for more details; in particular eq. 11 in that paper). We note however that the extreme N abundance in HE1327-2326 can be better fit in our model if we assume ^{14}N to be present in reasonable amounts in the PopIII-SNII ejecta. Interestingly, it has already been argued that ^{14}N could be produced in Pop III stars close to the $\sim 40M_{\odot}$ limit (Heger&Woosley 2010); this limit is lower when taking rotation into account (Joggerst et al. 2010). In our proposed picture, the extreme $[C/Fe]$ and $[O/Fe]$ values in HE1327-2326 is already indicative of a dsQN progenitor with mass at the high end of the $20M_{\odot} < M_{\text{prog.}} < 40M_{\odot}$ mass range. It is only fitting and natural to assume some ^{14}N already present in the PopIII-SNII ejecta. Of course, our model does not rule out the possibility of a companion at play in the case of HE1327-2326 given the initial CNO abundances we had to adopt for the fits.

5.1 Predictions

We now list some predictions of our model:

- An immediate implication of the astration-dsQN scenario suggested in this paper (see discussion in §4.3) is that the BBN ^7Li should be preserved in environments surrounding $> 40M_{\odot}$ Pop III stars. Pop II low-mass stars formed from clouds swept up by $> 40M_{\odot}$ PopIII-SNII should show imprints of elements synthesized in these massive Pop III stars and carry a BBN ^7Li abundance (in particular in warm low-mass stars formed these clouds). These stars would show a BBN $^6\text{Li}/^7\text{Li}$ ratio of $\sim 10^{-4}$ unlike the low-mass stars formed in clouds swept-up by dsQNe where, besides the $A(\text{Li}) \sim 2.2$ abundance of ^7Li from O-spallation, much higher values of $^6\text{Li}/^7\text{Li}$ are expected (see §5.3 and Figure 8 in Ouyed 2013). In addition, objects born from pristine clouds swept up by dsQNe should bear chemical imprints of spallation products as described

in this work. Thus we predict two distinct classes of low-mass Pop II stars.

- We found that in dsQNe with $8.3 \text{ days} < t_{\text{delay}} < 13 \text{ days}$ and $E_{\text{QN}} \geq 10 \text{ GeV}$, spallation in the C-layer resulted in ^7Li abundances exceeding meteoritic values ($A(\text{Li}) \sim 3.25$). The destruction of C at the expense of lighter elements in these dsQNe means that super-Li rich low-mass stars should also show relative depletion in Carbon. However, ^{12}C is also a by-product of spallation in the ^{16}O layer which suggest that not all super-Li candidates should appear carbon poor.

- In our model, QNe with $t_{\text{delay}} < 2 \text{ days}$ would lead to excessive (almost complete) destruction of ^{56}Ni . Thus, low-mass Pop II stars with much lower $[\text{Fe}/\text{H}]$ values than HMP stars should eventually be discovered if QNe with extremely short time delays occur in nature. However, these dsQNe are statistically extremely rare since they would originate from stars lying the closest to the black hole limit ($\sim 40M_{\odot}$): those forming the most massive NSs which undergo a QN phase transition with the shortest time delays.

- If some low-mass Pop II stars are made in binaries in the pristine cloud swept up by dsQNe with very short delays ($t_{\text{delay}} < 2.5 \text{ days}$ or $[\text{Fe}/\text{H}] < -6$), these should show excessive enhancement of CNO elements. The preservation of the original C and O (and N for the more massive dsQN progenitors) elements present in the PopIII-SNII ejecta, their production by spallation in the inner layers, and their accretion from the companion should lead to $[C/Fe]$, $[O/Fe]$ and $[N/Fe]$ values much in excess of those measured so far in carbon-enhanced, extremely metal-poor (CEMP) stars. The discovery of such stars, in particular if they show large $^6\text{Li}/^7\text{Li}$ ratios and large abundances of specific spallation products such as Fluorine and Scandium (see e.g. Figures 1, 12 and 13), would be a strong indication that our model might be a correct representation of extremely metal-poor Pop II stars and of the origin of the Spite plateau.

- We echo a previous point that besides being very neutron-rich, the QN ejecta is also rich in $A > 130$ elements (Jaikumar et al. 2007; see discussion in §6.4 in Ouyed 2013). A typical QN ejects on average $\sim 10^{-4}$ - $10^{-3}M_{\odot}$ of ejecta rich in $A > 130$ elements which is 10-100 times larger than in the case of a typical core-collapse SN ejects where on average $10^{-6}M_{\odot}$ in heavy elements is ejected (e.g. Woosley et al. 1994 and references therein). Since we estimate that on average QNe occur at a rate of 1 for every 100 core-collapse SNe (Leahy&Ouyed 2009; Ouyed et al. 2009a&b), this means that contamination by QNe should be equally important if not more dominant. These elements should be detectable in environments around low-mass Pop II stars with ^7Li abundance reflective of dsQNe. A possible site for the QN $A > 130$ tracers would be the ISM environment studied by Howk et al. (2012) in the Small Magellanic Cloud where the super-Li $A(\text{Li})$ value and the high $^6\text{Li}/^7\text{Li}$ measured, as we argued previously, might be indicative of a dsQN with C-spallation imprint.

- In this work and in Ouyed (2013), we argued that extremely metal-poor Pop II low-mass stars could have been born in pristine clouds swept up by primordial dsQNe. Furthermore, in Ouyed et al. 2009a we showed that primordial dsQNe provide ample ionizing photons per baryon to re-ionize the universe and provide the optical depth in the CMB of ~ 0.1 detected by WMAP. Thus according to our model, the end of the epoch of re-ionization should also coincide with the epoch of formation of Pop II low-mass stars. A notion which could be verified observationally.

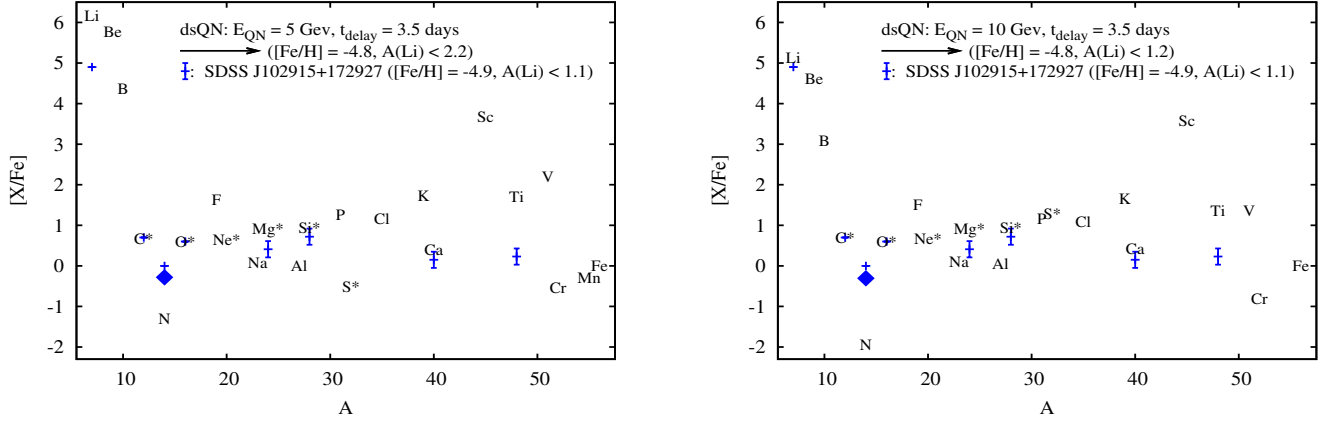


Figure 12. Relative abundances $[X/Fe]$ of sub-Fe spallation products (elements identified by their names) versus mass number A from simulations with $t_{\text{delay}} = 3.5$ days which resulted in $[Fe/H] \approx -4.8$. The CN enhanced nitrogen is shown by the filled diamond. Left and right panel are for QN neutrons with $E_{\text{QN}} = 5$ GeV and 10 GeV, respectively. SDSS J102915+172927's measured abundances are also shown, as plus (+) signs with the corresponding uncertainties, for a comparison (plus signs with no error bars are upper limits). We adopted measured abundances given in Caffau et al. (2011; see their Table 1) with an assumed upper limit for oxygen of $[O/Fe] \sim 0.6$. Best fits were found for initial abundances in mass of $M_{\text{Ni,SN}} = 0.1 M_{\odot}$, $M_{\text{S,SN}} = M_{\text{Si,SN}} = M_{\text{Mg,SN}} = M_{\text{Ne,SN}} = 0.01 M_{\odot}$, $M_{\text{O,SN}} = 0.04 M_{\odot}$ and $M_{\text{C,SN}} = 0.002 M_{\odot}$. The mass of the cloud swept by a dsQN was kept at $M_{\text{sw}} = 10^5 M_{\odot}$.

6 CONCLUSION

In this paper we made a case for QNe (specifically dsQNe) as sources of ${}^7\text{Li}$ in the pre-Galactic era. Lithium is produced by spallation on the PopIII-SNII ejecta material. For dsQNe with $t_{\text{delay}} > t_{\text{outer}} \sim 8.3$ days, an $A(\text{Li}) \sim 2.2$ ${}^7\text{Li}$ plateau results from spallation in the Oxygen layer matching observations of Spite&Spite (1982). We argue for a synergy between our model and the astration model of Piau et al. (2006). In the astration-dsQN scenario, the BBN is first processed/destroyed in the 20-40 M_{\odot} Pop III QN progenitor before it is restored to Spite values following spallation in oxygen layer of the PopIII-SNII ejecta. In our model, instabilities in the pristine cloud swept-up by the SN+QN (i.e. dsQN) ejecta should lead to the formation of low-mass stars with abundances reminiscent of those measured in old metal-poor dwarfs and in turn-off stars of globular clusters. According to our model, the most iron-poor stars likely formed from gas clouds swept up and enriched by dsQNe with very short delays. This effectively dissociates age from metallicity and thus calls for a paradigm shift in the current wisdom which seems to associate the iron content in stars increases with the cosmic age.

In today's universe, QNe should be associated with massive star (20-40 M_{\odot}) regions. At low redshift, dsQNe would manifest themselves as superluminous SNe (Ouyed et al. 2002; Leahy&Ouyed 2008; Ouyed et al. 2010) with a distinct "double-hump" light-curve – the first hump correspond to the core-collapse SN explosion proper and the second hump to the re-energization of the SN shell by the QN (see Ouyed et al. 2009b; Ouyed&Leahy 2012). Other imprints of dsQNe in today's universe have been suggested in the context of Ni-poor, Ti-rich SNe such as Cas A and in the context of SNe with peculiar chemical composition in general Ouyed et al. (2011). Interestingly, we find a similar range in t_{delay} (2 days $< t_{\text{delay}} < 20$ days) when fitting SLSNe light-curves (e.g. Ouyed et al. 2012; Kostka et al. 2012) and the chemical composition of some very peculiar SNe (Ouyed et al. 2011). This might be an indication (or plausibly a self-consistency check) on the universal nature of the physics underlying the QN explosion and of the mass of their progenitors. This range in t_{delay} combined with the estimate of the transient gravitational wave signal from QNe (Staff

et al. 2012) should lead to distinct dsQNe signatures in future Gravitational Waves detectors.

The existence of deconfined quark matter in the superdense interior of neutron stars is a key question that has drawn considerable attention over the past few decades. Here we have shown that the existence of the Spite plateau is an indication that quark matter does appear in the core of massive neutron stars and that it triggered the biggest explosions in the universe, namely the QNe. These QNe may also have played a role in the early universe by helping in its re-ionization (Ouyed et al. 2009a) and by triggering the formation of very low-metal Pop II stars (Ouyed 2013 and this work). Other implications to Cosmology have been discussed in Ouyed&Staff (2013).

ACKNOWLEDGEMENTS

I thank Jan Staff and Brian Niebergal for comments on the manuscript. The research of R.O. is supported by an operating grant from the National Science and Engineering Research Council of Canada (NSERC).

REFERENCES

- Abel, T., Bryan, G. L., & Norman, M. L. 2002, *Science*, 295, 93
- Adamów, M., Niedzielski, A., & Wolszczan, A. 2012, *Mem. S. A. It. Suppl.*, 22, 48
- Albornoz Vázquez, D., Belikov, A., Coc, A., Silk, J., & Vangioni, E. 2012, *Phys. Rev. D*, 86, 063501
- Angulo, C., Casarejos, E., Couder, M., et al. 2005, *ApJ*, 630, L105
- Aoki, W., Honda, S., Beers, T. C., et al. 2007, *ApJ*, 660, 747
- Arnett, D. W. 1996, *Supernovae and Nucleosynthesis*, Princeton Univ. Press. p. 188
- Asplund, M., Lambert, D. L., Nissen, P. E., Primas, F., & Smith, V. V. 2006, *ApJ*, 644, 229
- Beers T. C., Christlieb N., 2005, *Ann. Rev. A&A*, 43, 531
- Bodmer, A. R. 1971, *Phys. Rev. D*, 4, 1601
- Bonifacio, P., Molaro, P., Sivarani, T., et al. 2007, *A&A*, 462, 851
- Bonifacio, P., Monaco, L., Sbordone, L., Villanova, S., & Pancino, E. 2010, *IAU Symposium*, 268, 269

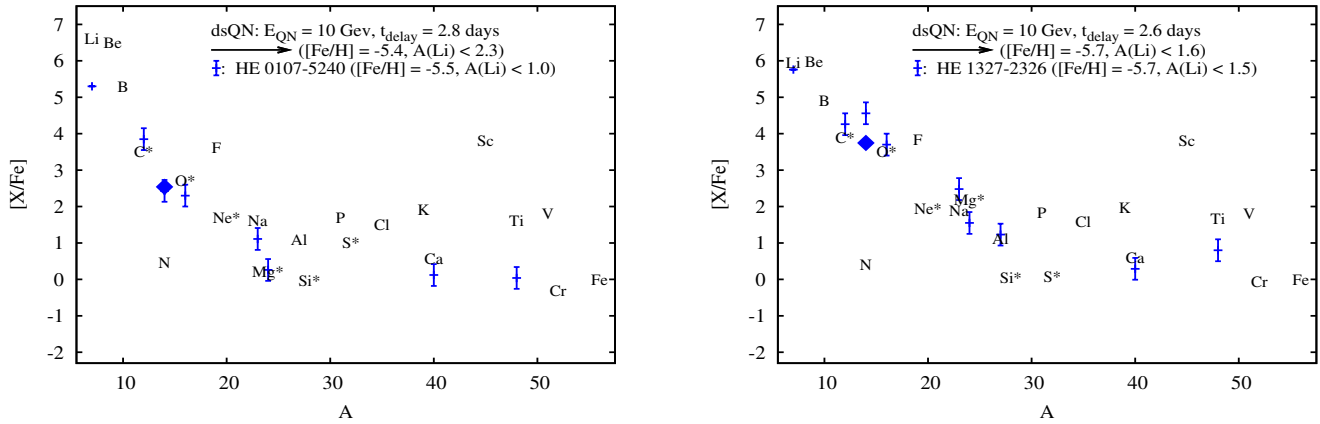


Figure 13. **Left panel:** Relative abundances $[X/Fe]$ of sub-Fe spallation products (elements identified by their names) versus mass number A from simulations with $t_{\text{delay}} = 2.8$ days and $E_{\text{QN}} = 10$ GeV which resulted in $[Fe/H] \approx -5.4$ and $A(Li) < 2.3$. The CN enhanced nitrogen is shown by the filled diamond. HMP-HE-0107-5240's measured abundances are also shown, as plus (+) signs with the corresponding uncertainties, for a comparison (plus signs with no error bars are upper limits). The fit was found for initial abundances in mass of $M_{\text{Ni,SN}} = M_{\text{S,SN}} = M_{\text{Si,SN}} = 0.01 M_{\odot}$, $M_{\text{Mg,SN}} = M_{\text{Ne,SN}} = 0.02 M_{\odot}$, $M_{\text{O,SN}} = 1.0 M_{\odot}$ and $M_{\text{C,SN}} = 3.0 M_{\odot}$. The CN enhanced nitrogen was obtained for a 1% enhancement factor; **Right panel:** Relative abundances $[X/Fe]$ of sub-Fe spallation products (elements identified by their names) versus mass number A from simulations with $t_{\text{delay}} = 2.6$ days and $E_{\text{QN}} = 10$ GeV which resulted in $[Fe/H] \approx -5.7$ and $A(Li) < 1.5$. HMP-HE-0107-5240's measured abundances are also shown, as plus (+) signs with the corresponding uncertainties, for a comparison. The fit was found for initial abundances in mass of $M_{\text{Ni,SN}} = M_{\text{S,SN}} = M_{\text{Si,SN}} = 0.01 M_{\odot}$, $M_{\text{Mg,SN}} = M_{\text{Ne,SN}} = 0.02 M_{\odot}$, $M_{\text{O,SN}} = 3.5 M_{\odot}$ and $M_{\text{C,SN}} = 3.5 M_{\odot}$. Both cases were run for an $M_{\text{sw}} = 10^5 M_{\odot}$ cloud swept by the dsQN. The measured abundances were taken from Norris et al. (2013).

Bromm, V., & Loeb, A., 2003, *Nature*, 425, 812
 Bromm, V., & Larson, R. B. 2004, *ARA&A*, 42, 79
 Caffau, E., Bonifacio, P., François, P., et al. 2011, *Nature*, 477, 67
 Caughlan, G. R., & Fowler, W. A. 1972, *Nature Physical Science*, 238, 23
 Cayrel, R., Depagne, E., Spite, M., et al. 2004, *A&A*, 416, 1117
 Chaboyer, B., & Demarque, P. 1994, *ApJ*, 433, 510
 Chakraborty N., Fields B. D., & Olive K. A., 2011, *Phys. Rev. D*, 83, 063006
 Charbonnel, C., & Talon, S. 2005, *Science*, 309, 2189
 Cherchneff, I., & Dwek, E. 2009, *ApJ*, 703, 642
 Christlieb, N., Bessell, M. S., Beers, T. C., et al. 2002, *Nature*, 419, 904
 Coc, A., Olive, K. A., Uzan, J.-P., & Vangioni, E. 2009, *Phys. Rev. D*, 79, 103512
 Coc, A., & Vangioni, E. 2010, *J. Phys. Conf. Ser.*, 202, 012001
 Cohen, J. G. et al. 2006, *AJ*, 132, 137
 Cyburt, R. H., Fields, B. D., & Olive, K. A. 2004, *Phys. Rev. D*, 69, 123519
 Cyburt, R. H., Fields, B. D., & Olive, K. A. 2008, *J. Cosmol. Astro-Part. Phys.*, 11, 12
 Cyburt R. H., Ellis J., Fields B. D., Luo, F., Olive K. A., & Spanos V. C., 2010, *J. Cosmol. Astropart. Phys.*, 10, 32
 Deliyannis, C. P., Demarque, P., & Kawaler, S. D. 1990, *ApJS*, 73, 21
 Deliyannis, C. P., Steinhauer, A., & Jeffries, R. D. 2002, *ApJ*, 577, L39
 Dunkley, J., Komatsu, E., Nolte, M. R., et al. 2009, *ApJS*, 180, 306
 Fields, B. D. 2011, *Annual Review of Nuclear and Particle Science*, 61, 47
 Frebel, A., Collet, R., Eriksson, K., Christlieb, N., & Aoki, W. 2008, *ApJ*, 684, 588
 Greif, T. H., Springel, V., White, S. D. M., et al. 2011, *ApJ*, 737, 75
 Heger, A., & Woosley, S. E. 2010, *ApJ*, 724, 341
 Howk, J. C., Lehner, N., Fields, B. D. & Mathews, G. J. 2012, *Nature*, 489, 121
 Iocco, F., Mangano, G., Miele, G., Pisanti, O., & Serpico, P. D. 2009, *Phys. Rep.*, 472, 1
 Itoh, N. 1970, *Prog. Theor. Phys.*, 44, 291
 Jaikumar, P., Meyer, B. S., Otsuki, K., & Ouyed, R. 2007, *A&A*, 471, 227
 Jedamzik, K., Choi, K.-Y., Roszkowski, L., & Ruiz de Austri, R. 2006, *Journal of Cosmology and Astro-Particle Physics*, 7, 7
 Jedamzik, K., & Pospelov, M. 2009, *New J. Phys.*, 11, 105028
 Joggerst et al. 2010, *ApJ*, 709, 11
 Keränen, P., Ouyed, R., & Jaikumar, P. 2005, *ApJ*, 618, 485

Klessen, R. S., Glover, S. C. O., & Clark, P. C. 2012, *MNRAS*, 421, 3217
 Koch, A., Lind, K., Thompson, I. B., & Rich, R. M. 2012, *Mem. S. A. It. Suppl.*, 22, 79
 Kohri, K., & Santoso, Y. 2009, *Phys. Rev. D*, 79, 043514
 Kostka, M., Koning, N., Ouyed, R., Leahy, D., & Steffen, W. 2012, *arXiv:1206.7113*
 Komatsu, E., Smith, K. M., Dunkley, J., et al. 2011, *ApJSuppl.*, 192, 18
 Lambert, D. L. 2004, in *AIP Conf. Proc.* 743, *The New Cosmology*, ed. R. E. Allen, D. V. Nanopoulos, & C. N. Pope (New York: AIP), 206
 Larson, R. B. 1998, *MNRAS*, 301, 569
 Larson, D., Dunkley, J., Hinshaw, G., et al. 2011, *ApJ Supplement Series*, 192, 16
 Leahy, D., & Ouyed, R. 2008, *MNRAS*, 387, 1193
 Leahy, D., & Ouyed, R. 2009, *Advances in Astronomy*, 2009
 Limongi, M., & Chieffi, A. 2012, *ApJ Supplement Series*, 199, 38
 Loeb, A., Ferrara, A., & Ellis, R. S. 2008, *First Light in the Universe*, ed. Loeb, A., Ferrara, A., & Ellis, R. S.
 Machida, M. V., Tomisaka, K., Nakamura, F., & Fujimoto, M. Y. 2005, *ApJ*, 622, 39
 McCray R., 1985, in *Spectroscopy of Astrophysical Plasmas*, edited by A. Delgarno & D. Layzer, p. 270
 McWilliam, A. 1997, *ARA&A*, 35, 503
 Meléndez, J., & Ramírez, I. 2004, *ApJ*, 615, L33 (MR04)
 Michaud, G., Fontaine, G., & Beaudet, G. 1984, *ApJ*, 282, 206
 Monaco, L., Villanova, S., Bonifacio, P. et al. 2012, *A&A*, 539, A157
 Mucciarelli A., Salaris M., Lovisi L., Ferraro F. R., Lanzoni B., Lucatello S., Gratton R. G., 2011, *MNRAS*, 412, 81
 Nakamura, F. & Umemura, M. 2002, *ApJ*, 569, 549
 Niebergal, B., Ouyed, R., & Jaikumar, P. 2010, *Phys. Rev. C*, 82, 062801
 Nissen P.E., Akerman C., Asplund M., Fabbian D., Kerber F., Kaufl H.U., Pettini M., 2007, *A&A* 469, 319
 Norris, J. E., Yong, D., Bessell, M. S., et al. 2013, *ApJ*, 762, 28
 Nozawa, T., Kozasa, T., Umeda, H., Maeda, K., & Nomoto, K. 2003, *ApJ*, 598, 785
 Nozawa, T., Kozasa, T., & Nomoto, K. 2012, *ApJ*, 756, L35
 Ouyed, R., Dey, J., & Dey, M. 2002, *A&A*, 390, L39
 Ouyed, R., Rapp, R., & Vogt, C. 2005, *ApJ*, 632, 1001
 Ouyed, R., & Leahy, D. 2009, *ApJ*, 696, 562
 Ouyed, R., Pudritz, R. E., & Jaikumar, P. 2009a, *ApJ*, 702, 1575

- Ouyed, R., Leahy, D., & Jaikumar, P. 2009b, in Proceedings for "Compact stars in the QCD phase diagram II (CSQCD II)", May 20-24, 2009, KIAA at Peking University, Beijing- P. R. China [arXiv:0911.5424]
- Ouyed, R., Kostka, M., Koning, N., Leahy, D. A., & Steffen, W. 2012, MNRAS, 423, 1652
- Ouyed, R. et al. 2011, Physical Review Letters, 107, 151103
- Ouyed, R. 2013, MNRAS, 428, 236
- Ouyed, R., & Staff, J. 2013, Research in Astronomy and Astrophysics, 13, 435
- Ouyed, R., & Leahy, D. 2013, submitted [arXiv:1202.2400]
- Piau L., Beers T. C., Balsara D. S., Sivarani T., Truran J. W., Ferguson J. W., 2006, ApJ, 653, 300
- Piau, L. 2008, ApJ, 689, 1279
- Pinsonneault, M. H., Deliyannis, C. P., & Demarque, P. 1992, ApJS, 78, 179
- Pinsonneault, M. H., Steigman, G., Walker, T. P., & Narayanan, V. K. 2002, ApJ, 574, 398
- Prantzos, N. 2007, Space Sci. Rev., 130, 27
- Ryan, S. G., Norris, J. E., & Beers, T. C. 1999, ApJ, 523, 654
- Richard, O., Michaud, G., & Richer, J. 2005, ApJ, 619, 538
- Salaris, M., & Weiss, A. 2001, A&A, 376, 955
- Sbordone, L., Bonifacio, P., Caffau, E., et al. 2010, A&A, 522, A26
- Sbordone, L., Bonifacio, P., & Caffau, E. 2012, Mem. S.A.It., Vol. 75, 282
- Schneider, R., Omukai, K., Inoue, A. K., & Ferrara, A. 2006a, MNRAS, 369, 1437
- Schneider, R., Salvaterra, R., Ferrara, A., & Ciardi, B. 2006b, MNRAS, 369, 825
- Shigeyama, T., & Tsujimoto, T. 1998, ApJ, 507, L135
- Silvia, D. W., Smith, B. D., & Shull, J. M. 2010, ApJ, 715, 1575
- Spite, F., & Spite, M. 1982, A&A, 115, 357
- Spite, M., Cayrel, R., Plez, B., et al. 2005, A&A, 430, 655
- Spite, M., Caffau, E., Andrievsky, S. M., Korotin, S. A. et al. 2011, A&A 528, A9
- Spite, M., Spite, F., & Bonifacio, P. 2012, Memorie della Societa Astronomica Italiana Supplementi, 22, 9
- Staff, J. E., Ouyed, R., & Jaikumar, P. 2006, ApJ, 645, L145
- Staff, J. E., Jaikumar, P., Chan, V., & Ouyed, R. 2012, ApJ, 751, 24
- Suda, T., Aikawa, M., Machida, M. N., Fujimoto, M. Y., & Iben, I., Jr. 2004, ApJ, 611, 476
- Talon, S., Kumar, P., & Zahn, J.-P. 2002, ApJ, 574, L175
- Talon, S., & Charbonnel, C. 2004, A&A, 418, 1051
- Terazawa, H., 1979, INS-Report-338, University of Tokyo
- Tumlinson, J., Venkatesan, A., & Shull, J. M. 2004, ApJ, 612, 602
- Tumlinson, J. 2007, ApJ, 665, 1361
- Umeda, H. & Nomoto, K. 2002, ApJ, 565, 385
- Umeda, H., & Nomoto, K. 2005, ApJ, 619, 427
- Vauclair, S. 1988, ApJ, 335, 971
- Vogt, C., Rapp, R., & Ouyed, R. 2004, Nuc. Phys. A, 735, 543
- Wise, J. H., & Abel, T. 2007, ApJ, 671, 1559
- Witten, E. 1984, Phys. Rev. D, 30, 272
- Woosley, S. E., Wilson, J. R., Mathews, G. J., Hoffman, R. D., & Meyer, B. S. 1994, ApJ, 433, 229